SSC-219

The Superconducting Super Collider

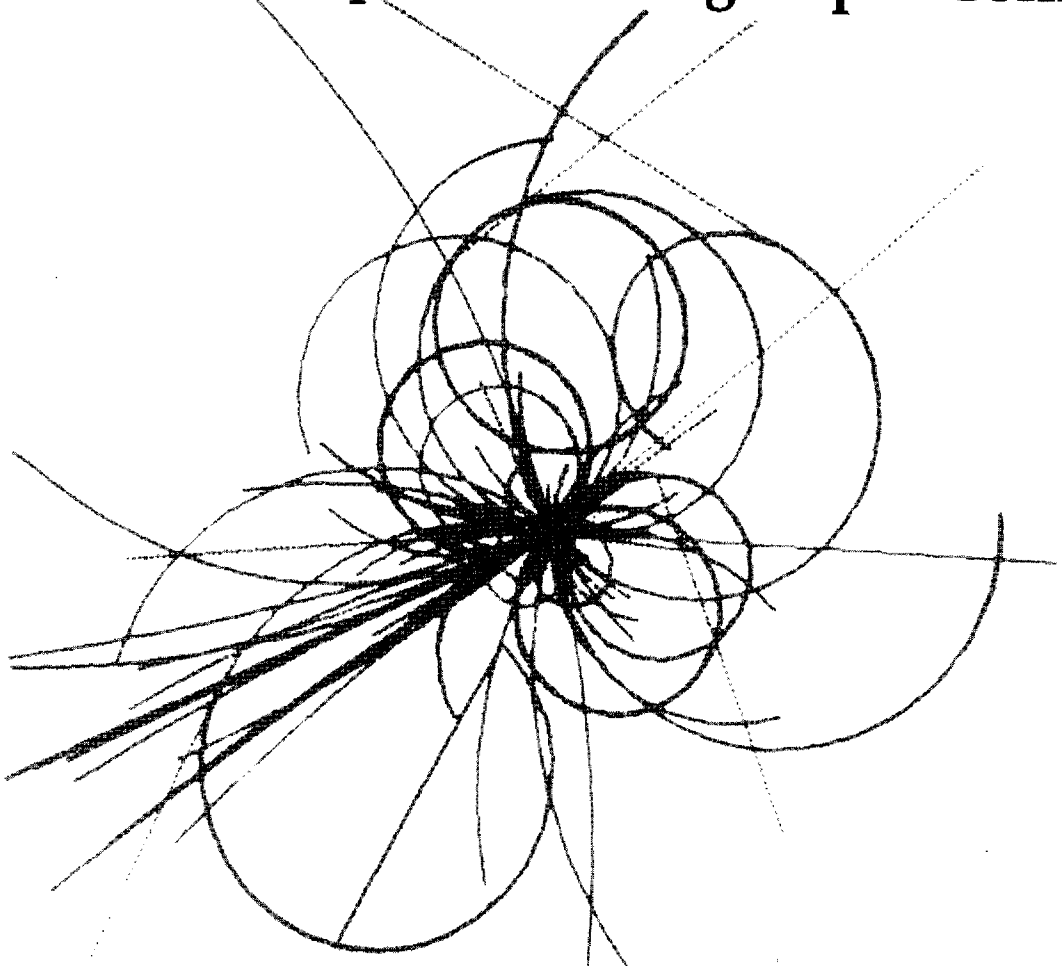

EMPACT—An Alternative Approach to a High P_T SSC Experiment

Michael Marx
SSC Central Design Group

May 1989

SSC-219

EMPACT—An Alternative Approach to a High P_T SSC Experiment

Michael Marx
SSC Central Design Group,* c/o Lawrence Berkeley Laboratory, Berkeley, CA 94720
and
Physics Department, State University of New York, Stony Brook, NY 11794

May 1989

*Operated by Universities Research Association for the U. S. Department of Energy

Introduction

A survey of high P_T detector concepts advanced for the SSC reveals two striking facts—first, the scale of most detectors is set by the muon detection system; and second, that the performance of these muon systems is limited in comparison to electron or jet capabilities, either in resolution or in rapidity acceptance. I propose here an alternative concept for an SSC experiment which will provide enhanced muon performance at a level to that obtainable through calorimetric means for electrons and jets, while drastically reducing the tonnage of the experiment.

2. SSC Physics

The primary motivation for constructing a 40 TeV hadron collider is to uncover the mechanism for symmetry breaking in the electroweak sector—generating the mass of the W and Z° (Ref. 1).

While the source of this breaking may be controversial, the mass scale below which it must manifest itself is not. All theories indicate that strong interactions of the longitudinal components of the vector bosons, i.e.,

$$W_L^+ W_L^- \rightarrow Z_L^o Z_L^o$$

must increase, violating unitarity in the 1-2 TeV range unless some mechanism suppresses it. This situation exactly parallels the previous need for the W and Z°, which prevented the weak cross sections from violating unitarity around 300 GeV.

The simplest standard model, predicts the existence of a Higgs singlet, H°, whose width increases like M_H^3, and decays predominantly (for $M_H > 2M_Z$) into

vector boson pairs. Supersymmetric models, which have profound implications for unification of all forces, predict partners for the known objects and also new W′ and Z′ bosons at higher mass, all of which have well defined interactions and decay, but unknown mass. Many of the predicted particles produce W's and Z's in their decay chains, as well as decays characterized by the absence of leptons in the presence of jets and missing P_T.

In addition to the exploration of symmetry breaking, the SSC will be concerned with searches for new heavy quarks (including top, if it has not been found at the TeVatron) and leptons. Again one finds in the signatures for these particles vector bosons (i.e. $t \rightarrow Wb$), leptons, jets and missing P_T.

There is a great deal of work that has been done on these subjects (see, for example, References 1 and 2, and references therein). My conclusions in trying to assimilate this information are twofold:

1) The vector bosons, $W^{\pm}$ and Z°, and hence their decay products — e, μ, jets and ν, must be well measured and identified for a successful attack on SSC physics.

2) Despite copious production of many of the objects of interest, the clear signatures are usually from minority decay modes and must be extracted from large backgrounds.

Thus one is driven to as broad an approach to these signatures as possible, namely to study decay modes to both electrons and muons as well as quarks (jets) to provide confirmation of new signals in several channels. Electron capabilities also ensure that isolated photons can also be studied, leading to general studies of vector boson couplings. In addition, given the levels of predicted backgrounds, there will be a premium on good resolution which, for many studies, translates

directly into enhanced signals-to-noise ratios. One should provide the maximal possible solid angle to increase statistics and the detector should strive for maximal uniformity in detection techniques, in both rapidity and azimuth, to provide the best possible understanding of background.

The challenge is then to design a detector which provides these features. In Table I, I list a set of goals for such a SSC detector: it is primarily to measure electrons, jets and muons to a precision of 2 percent at 500 GeV, over a rapidity range of $|\eta| > 3$, and to measure missing P_T at the limit set by produced neutrinos from light quark decay.

Most detectors described in workshops (Ref. 3) achieve these goals for electrons, jets and missing P_T, but fall short on muon performance. In the following sections, I will explore the need for enhancing muon performance and discuss the reasons for the limitations for muons.

The impact of angular acceptance for the Higgs signals is shown in Figures 5 and 6 (Ref. 6) Here the acceptances for two leptons (signalling reaction 2) or four leptons (reaction 1) are shown as a function of minimum angle of coverage. The solenoidal detectors (Ref. 7 and Ref. 8) have good resolution which falls off sharply around 30-40°, resulting in signal losses of more than a factor or two!

Perhaps the best example of the need for both good acceptance and good resolution is available in the detection and identification of a new Z′. Several Z′s arise naturally in superstring inspired supersymmetric models. For example, one appears as E(6) breaks to SO(10) and another arises as SO(10) reduces to SU(5). Rosner (Ref. 9) has shown that the distinguishing feature of the various possible physical manifestations of the Z′ is the lepton asymmetry, which is a strong function of the Z′ mass and is largest at high rapidity. The asymmetry as a function of rapidity, as shown in Figure 7, indicates the importance of measurements at or beyond $y = 2$ (below 20°). Figure 8 shows the lepton acceptance from Z′ decay for various Z′ masses (Ref. 6). Adeva et al. (Ref. 10) have studied the impact that resolution has on the measurement of the asymmetry. Figure 9 shows the effect of measurement using iron toroids; Figure 10 shows the expected and "measured" asymmetry as a function of mass at large rapidity. The conclusion is that solenoids cannot be used to measure asymmetries and iron toroids do not have sufficient resolution to distinguish between different hypotheses.

Finally, it should be noted that detection and precision measurement of muons is particularly important, because of the possibility of finding muons within a jet core, which is impossible for electrons.

4. Limitations on Solenoids and Iron Toroids

Two geometries for solenoidal detector configurations are shown in Figure 11 (Large Solenoid Detector (LSD) (Ref. 7)) and Figure 12 (L3 + 1 (Ref. 8)). The expected momentum resolution for muons for the LSD is shown in Figure 13 for $\eta = 0$ (90° to the beams). It is seen that below p = 350 GeV/c the solenoidal tracking provides better resolution, and above this the resolution is determined by measurements in the iron flux return and toroids. Figure 14 shows how the resolution of the solenoid varies with rapidity. The P_T resolution is constant until particles no longer traverse the full field length, at which point the resolution deteriorates like $1/\sin^2\theta$. Similar behavior is shown for the external solenoid of L3 + 1, as shown in Figure 15. It is possible to increase the rapidity range by lengthening the solenoid as shown in Figure 12 (Ref. 11).

The implications of this limit in acceptance was shown in Figures 5 and 6 (Ref. 6), which showed the acceptance for the leptons from one or both Z's from Higgs decay. The big solenoids described above have cutoff acceptance angles between 30 and 40 degrees. This implies the need for poorer resolution iron measurements for the smaller angle muons, while for electrons it implies the need for different techniques and background considerations in small and large angle regions. As stated before, for new Z's the solenoidal acceptance precludes asymmetry measurements, which are only significant for $|\eta| > 2$.

There has been considerable effort devoted to studies of momentum resolution for muons in iron spectrometer systems. In these systems the bending in almost saturated iron competes with the multiple scattering, giving rise to a constant momentum resolution (until, at high energy, detector resolutions dominate) which improves as the square root of the iron thickness. These are shown

schematically in Figure 17, and basically provide measurements inside the iron ("sagittas") combined with measurements of incoming or outgoing directions. Typical achievable resolutions are shown in Figure 18 (Ref. 12).

These calculations do not consider the effects of muon interactions in material which become increasingly significant as muon energies rise. There is the possibility of catastrophic energy losses by deep inelastic or pair production processes, which lead to significant tails on the muon energy loss. More problematic for tracking considerations is the probability of radiating a photon by bremsstrahlung, which can initiate an electromagnetic shower. Where these showers overlap the muon track they effectively prevent precision tracking at that point. Figure 19 (Ref. 13) shows the probability of an unaccompanied muon exiting 1 m of steel or uranium. One sees that at 1 TeV, 25 percent of the muons exiting a calorimeter will be obscured and 20 percent of muons exiting a steel segment will be lost. One can infer from this, for example, that although one can achieve 15 percent muon resolution at 1 TeV in iron (Fig 18) the tracking efficiency may only be 50 percent, decreasing rapidly with energy. While one can improve overall efficiency inside iron by more frequent sampling, it is difficult to improve the efficiency for entrance and exit points.

This problem is reduced in a geometry in which muons are measured in air after passing through absorber material (Ref. 8). In this case, showers accompanying the muon are fanned out by the field, offering the possibility of finding the muon by extrapolating back the clean muon hits. This is shown in a simulated event in Figure 20 (Ref. 14). Innocente has shown that it is also possible to reconstruct the initial muon energy by tracking back through the absorbers to the vertex (Ref. 15). Measurement of momentum at levels desired in air is limited only by the available field integral and chamber resolution.

5. EMPACT

Two points emerge from all these considerations. First, in order to obtain the best possible precision in muon momentum measurements at the SSC one should measure the magnetic deflection in air rather than in iron. At the energies of interest, one would then be limited only by available field length and the resolution and number of measurements. Second, the solenoidal field configuration is not an optimal choice for hadron physics where much of the acceptance is outside of the good field regions. While this is particularly clear for the case of muon measurements, the drop in solenoidal acceptance also forces changes in the required technology and consequent nonuniformity in the measurement of electrons and jets. Jet algorithms, jet sizes, electron identification and background determination will all change at $|\eta| \sim 1.5$.

A possible solution of the muon problem, is a spectrometer constructed from superconducting air core toroids. This provides the possibility of generating a purely azimuthal field always perpendicular to the trajectories, and by simple arrangement of the currents one can create a field integral which increases like $1/\sin\Theta$, ensuring a P_T resolution independent of η.

The use of toroids in a hadron collider environment has been previously discussed (Ref. 16), but the geometry here is one of distributed, rather than lumped, coils. The configuration envisioned is shown in Figure 21. It consists of a central and two end toroids, each with 8 independent octagonal coils, with 3m of clear space for tracking chambers between inner and outer coils.

As an example of possible parameters, consider the central toroid with inner coil at 3m and outer coil at 6m. To achieve a field integral of 4.2 Tm at 90°, the total current is 3×10^7A turns, resulting in 2T at the inner conductors. With

similar currents, and 3m depth, the end toroid would have about 23 Tm at 5° ($\eta = 3$) and 6T at the inner conductors. This can be tuned by adjusting the depths of the end toroids. (See Appendix A.) The forces in these magnets are large, but the current densities can be relatively low and, since muons are being measured, structural coil support can be substantial. The coils are completely independent and space can be provided between supports for access, services and support for the internal detectors. It should be noted that there is a large body of expertise in superconducting toroids in the field of (warm) fusion energy, and the initial reaction of some experts to the present concept has been encouraging (Ref. 17).

The total weight of such a system of toroids is estimated at 1500 tons. This should be contrasted with the muon systems of other designs which require ten to twenty times this weight in iron.

This toroidal system can be used to achieve the goals for an SSC detector specified in Table 1. A possible realization of such a detector, EMPACT (Electrons, Muons, Partons with Air Core Toroids), is shown schematically in Figure 22. This detector consists of an inner tracking system surrounded by a precision hermetic calorimeter which is enclosed by the toroidal system and its precision tracking chambers. Because of the toroidal geometry, there is no magnetic field in either the inner tracking or calorimetric volume, although addition of a field is not precluded.

The primary functions of the tracking system are to aid in electron identification and background suppression, vertex determination to improve muon measurements, identification of multiple interactions, and general determination of event topologies and multiplicity. For electron signals, the primary concerns are establishment of isolation, suppression of pair conversions

through dE/dx measurements, and identification of charged-neutral overlaps through track matching. The latter two issues are primarily of concern for backgrounds to low P_T electrons.

Candidate technologies for the tracking include silicon pad tracking devices with pads matched to calorimeter towers; and/or azimuthal straw chambers which might incorporate TRDs.

The calorimetry is the crucial element of EMPACT. It must provide precision measurement of electrons, jets and missing P_T. The primary means of electron identification comes from determination of the transverse and longitudinal shower shape. The calorimeter should be able to reconstruct jet-jet masses to reconstruct vector bosons from Higgs decays (Ref. 18). It is also to be used as an aid in the muon trigger and to reconstruct muon energy losses. Finally the calorimeter is designed to provide sufficient absorber to allow detection, triggering and measurement of muons outside of the calorimetry.

At present, liquid argon with uranium absorber is the leading candidate for the calorimetry. Recent engineering work has demonstrated a "proof of principle" for a system that satisfies the requisite hermeticity requirements (Ref. 19). The model is shown in Figure 23 and the resolution as a function of rapidity is shown in Figure 24. While the effects of cryostat walls are visible, the overall impact on missing P_T is negligible (Ref. 20). Work at a recent workshop has also shown that the response time of such a calorimeter is adequate for the SSC (Ref. 21). Finally, measurements from two groups have shown that a liquid argon-uranium combination can yield a compensated calorimeter (Ref. 22). A second possibility for the calorimetry is based on the uranium scintillator technology

exploited at ZEUS (Ref. 23). This has some advantages but the main concern is deterioration due to radiation damage in the SSC environment.

Directly outside the calorimetry is the system of superconducting toroids. Within the volume between the inner and outer conductors a sophisticated system of precision tracking must measure the deflection of muons in the field. This system must also provide sufficient pattern recognition to find the muon track amidst hadron punchthrough and bremsstrahlung showers, which will be fanned out by the field. Beyond the outer coil, cruder tracking elements will provide the high P_T trigger and at high momentum can improve the resolution by extending the lever arm for measurement (multiple scattering in the outer coil is less than 5 percent of the magnetic bend).

An existence proof for this type of tracking is provided by the L3 Collaboration (Ref. 8) who have achieved 136 μm single point resolution. Using similar precision drift chamber techniques, it will be possible to obtain 2 percent resolution on the 0.9 mm sagitta of a 500 GeV muon at 90°; this will require 60 measurements at the ends of the track and 120 at the center. It may be possible to significantly reduce the number of measurements by using a solid or liquid radiator and a chamber with photosensitive gas (TMAE), which will measure the center of a distribution of Cerenkov photons produced in the radiator. Similar techniques (on a much smaller scale) have been proposed for a CERN experiment (Ref. 24) and claim to achieve a resolution on the trajectory of $1.6/\sqrt{N}$ times the single point resolution, where N is the number of detected photons. The total anticipated area for such chambers is 2500 m^2. Figure 22 also indicates a forward system to measure energy and muons out to $\eta = 5$. The requirements of such a system in any 4π detector are not yet clear, but it is possible to extend the toroid concept to this region.

This entire detector is estimated to weigh around 7500 tons. It is possible therefore to envision that this detector can be assembled in a garage and be moved on a platform (similar to the 5500 ton D0 detector) into the interaction region. This has enormous benefits for scheduling logistics, during assembly, and later for detector servicing and upgrades.

Triggering and data acquisition for this experiment are expected to be no more difficult than that for any of the previously discussed 4π detectors.

6. Advantages of Non Magnetic Tracking

A key element in the design of EMPACT is the absence of magnetic field in both the inner tracking and calorimetry regions. While it may be argued that a detector cannot be improved by removing a possibly useful feature, in the case of a hadron collider detector the cost of including a magnetic field significantly exceeds the advantages it may offer.

Several designs have been considered for a solenoidal field. These include large coils outside the calorimetry (Ref. 7 and Ref. 8), thin coils inside (Ref. 11) and high field compact designs (Ref. 25). The large coils require 20,000 tons of iron to return the flux and have significant influence on the calorimeter technology. For example, a magnetic field may preclude the use of transformers for capacitance matching in liquid argon or photo tubes for viewing scintillators. Support of the thousands of tons of calorimetry inside a large coil is a technological challenge and the coil itself occupies almost a meter of radial space increasing the size and cost of the external muon system. The high field and thin coil designs impact the hermeticity of the calorimetry because of the need for magnet

supports and services. In addition, such designs still have significant, albeit reduced, fields in the calorimetry volume.

The field itself detracts from calorimeter performance by spreading out low momentum component of jets, degrading the intrinsic resolution of a good calorimeter by a factor of two (Ref. 26). The field also causes low momentum particles to spiral, adding to the number of track hits, increasing the possibility of secondary interactions, and confusing the interpretation of energy depositions in the end calorimeters.

An advantage cited for use of magnetic tracking is the capability of determining the sign of electrons. As discussed earlier for the solenoid geometry, this can only be done for $|\eta| < 1.5$ or for half of the angular range of products from decay of heavy objects. In EMPACT the muon sign will be determined over the full solid angle of interest and, since the resolutions will be similar, backgrounds and signals can be compared for electron and muons. The only high P_T physics issues that depend critically on the sign are the asymmetry measurements of new Z′ decays, and evidence for production of like-sign W pairs. As discussed previously, the Z′ measurements need to be performed at high rapidity, beyond the acceptance range of most solenoids. Even with sign measurements, the W^+W^+ signal will be hard to establish because of two missing neutrinos. Figure 25 shows the two lepton acceptance for high P_T W pairs (Ref. 6) and indicates that this is also unlikely to be accomplished with electrons using a solenoid configuration.

Magnetic tracking also provides additional electron identification through comparison of electron energy in the calorimetry with the measured momenta. Estimates (Ref. 7) indicate this provides only a factor of about three in additional discrimination over that obtained by calorimetry alone, the method is only useful

for $|\eta| < 1.5$ and, more importantly, only for electron P_T less than 50 GeV, after which point the resolution for momentum becomes worse than the resolution of the calorimeter. The magnet also aids in suppressing electron backgrounds from photon conversions as well as from overlaps of charged and neutral pions. However, these backgrounds are important at low P_T.

Magnetic fields also permit measurements of jet fragmentation functions, which provide data for correcting of jet dispersion (caused by the magnet), and non-linearities in calorimetry response (caused by lack of compensation). These types of measurements will likely be limited to low luminosity and P_T, and the information could in principle be obtained from separate smaller experiments or from e^+e^- data in conjunction with QCD models. The measurement of particle momenta, also provides a valuable in situ calibration of the calorimeter, limited to P_T where the magnetic and calorimetric resolutions are comparable.

Magnetic analysis provides the opportunity to reconstruct secondary decay vertices, which may yield an additional handle on new physics. It is in respect to this kind of intangible asset of redundancy and additional information that the magnetic field has its strongest appeal.

The absence of magnetic field allows optimization of tracking and calorimetry in the EMPACT design. All trajectories are straight, resulting in simpler tracking and calorimetric analysis. Electron identification is accomplished by a highly segmented calorimeter augmented with tracking /dE/dx/TRD information to reduce hadron misidentification. Electrons and jets can be measured over the full solid angle using the same techniques. This homogeneity and uniformity maximizes uniformity of response to signal and backgrounds. Calibration can be accomplished using the copious Z° (and W) signals to provide

an absolute energy scale by reconstructing the mass. Decay electrons from the Z°s are distributed in energy over most of the dynamic range of the calorimeter. The lack of a magnet permits a mechanical design and support of the calorimetry and tracking which is simpler, less costly, and probably more hermetic. Finally we note that the upgraded UA2 is highly competitive with the magnetic detectors (CDF and UA1).

7. Development Issues

The EMPACT concept has many attractive features. However, the concept must be evaluated quantitatively, and the appropriate detector technologies addressed before it can be considered a realistic alternative to previous designs. The major issues are

- The feasibility of fabricating superconducting air core toroids of this size. Initial engineering effort should set the scale for costs, schedule and mechanical support systems. It is estimated that this can be accomplished within three months (Ref. 27). For the longer term, one needs to optimize the conductor shape and currents to provide the requisite field integral for doing SSC physics.
- Technologies for large area precision tracking of muons must be developed. Tracking in the $1/r$ toroidal field and effects of field non-uniformities must be considered carefully.
- Backgrounds for muon detection and triggering must be correctly modelled to determine if additional absorber is needed, and to ensure that tracks can be found and measured in the background sea of low P_T hadron punchthrough and bremsstrahlung showers.

- The utility of measuring muon trajectories outside of the toroids and the precision needed for determining the production vertex must be established.
- The minimum radius required to begin calorimetry must be examined in light of the physics goals. This sets the overall scale for the experiment and directly impacts the currents required in the toroids. For example, moving the central toroid out 1m can be compensated by raising the current by 25 percent to maintain the same field integral.
- Finally, there is the full list of R&D issues faced by all other designs, including specification and development of tracking and calorimetry technologies as well as a more detailed specification of a complete set of physics goals in terms of their requirements in detector performance. The single most important issue is to set the minimum P_T for clean lepton identification—clearly, the higher this can be set without loss of physics, the simpler the detector can become.

8. Conclusion

The EMPACT detector presented here provides an alternative to previous SSC design concepts for 4π high P_T physics. It is unique in its ability to provide muon measurements at the level of calorimetric electron (or photon) and jet resolution. The air-core toroids equalize the mass reach for electron and muon decay channels of heavy Higgs, and provide unique capability for distinguishing the character of new Z's from their decay asymmetry measurements. It provides powerful tools for the study of most high P_T SSC phenomena, from the studies of new particles to the production, decays and interactions of the old vector bosons.

The configuration of detectors provides uniformity of technology over the full solid angle of interest, for muons as well as electrons and jets. The geometry permits the precision tracking of muons in relatively low multiplicity environment, and offers the possibility of extending the range of measurement beyond the field, if dictated by new physics.

From purely logistical considerations, EMPACT eliminates tens of thousands of tons of steel for flux return and muon spectrometers, and this will enable the entire detector to be moved on or off the beam. Because of the modular nature of the coils, there is minimal interaction with the calorimeter and tracking supports, and thus can provide access and services to the internal detectors.

There is, of course, a great difference between an attractive concept and a realistic detector design. EMPACT offers several clear advantages and work must begin soon if a competitive 4π detector for the SSC is to emerge from these ideas.

Acknowledgements

I would like to thank the SSC Central Design Group and especially M. Gilchriese for their support. G. Trilling and cohorts of the Solenoid Study Group at LBL provided much of the stimulation for the ideas presented here. I would like to acknowledge valuable discussions with E. Wang, R. Cahn, and especially F. Paige for ELMUD. It is a pleasure to acknowledge B. Pope for educating me on the advantages of toroidal magnets. It is obvious that without the resource of the work done and reported by many people at the Snowmass and Berkeley workshops this present work could not have been accomplished.

Finally, I thank T. Ferbel and D. Flattery for their critical reading of the manuscript.

Appendix A

Toroidal Parameters and Performance

Figure 26 shows an idealized distribution of current elements defining a toroidal system with definition of physical parameters. Note that central and end systems can be arbitrarily separated by introducing additional opposing current legs without changing field distributions.

The purely azimuthal magnetic field is given by

$$B(\text{Tesla}) = 2 \times 10^{-7} \frac{NI\ (\text{Amps})}{R(\text{meter})}$$

Thus the product B R is a constant for the system. As an example, for the toroids discussed for EMPACT, NI = 3×10^7 Amps and BR = 6 Tesla - meters.

Of interest for this system is the variation of the field integral with angle, and the sagitta, which is proportional to the path times the field integral. This is tabulated below

	$\int Bdl$	$L \int Bdl$
90°	$BR\, ln \frac{R_o}{R_i}$	$BR\,(R_o - R_i)\, ln \frac{R_o}{R_i}$
Central	$\frac{BR}{\sin\theta}\, ln \frac{R_o}{R_i}$	$\frac{BR\,(R_o - R_i)}{\sin^2\theta}\, ln \frac{R_o}{R_i}$
Ends	$\frac{BR}{\sin\theta}\, ln \frac{Z_o}{Z_i}$	$\frac{BR\,(Z_o - Z_i)}{\sin\theta\ \cos\theta}\, ln \frac{R_o}{R_i}$

The stored energy for the central toroid is given by

$$U = 2.5\, L\, (BR)^2\, ln \frac{R_o}{R_i}$$

For EMPACT this results in 930 Mega Joules for the central and 480 MJ for each end. For comparison the solenoid of the LSD design (Ref. 7) has a stored energy of 1200 MJ.

References

1. "Physics at the SSC — Introduction and Overview", G. L. Kane, *Proceedings of the 1986 Summer Study on the Physics of the Superconducting Supercollider,* edited by R. Donaldson and J. Marx, Snowmass, Co (1986) (hereafter SNM 86), p. 7 "Physics at Large Traverse Momenta", I. Hinchliffe, *Proceedings of the Workshop on Experiments, Detectors, and Experimental Areas for the Supercollider,* edited by R. Donaldson and M. Gilchriese, Berkeley (1987) (hereafter BERK 87), p. 1.

2. "Detecting the Heavy Higgs at the SSC", R. N. Cahn, et. al., BERK 87, p. 20.

3. "Summary and Comparison of High P_T Detector Concepts", R. J. Cashmore et al., BERK 87, p. 301

4. "Higgs to Four Leptons at the SSC", E. M. Wang, et al., LBL - 26561, (1988).

5. "Heavy Top Quark Production as a Background in the Search for the Higgs Boson", G. Herten, BERK 87, p. 103.

6. "Leptonic Angular Acceptance", D. Carlsmith et al., SNM 86, p. 431.

7. "Report of the Large Solenoid Detector Group", BERK 87, p. 340.

8. "Muon Spectrometers — Report of the Detector Subgroup", BERK 87. p. 525.

9. "New Contributions to Forward Backward Asymmetries in Hadronic Lepton Pair Production", J. L. Rosner, SNM 86, p. 213.

10. "New Z Bosons at the SSC", B. Adeva et al., SNM 86, p. 257.

11. "A Design of a Small Thin Superconducting Solenoid for a General Purpose 4π Detector at the SSC", A. Yamamoto et al., KEK preprint (1989).

12. "SSC Muon Detector Group Report", SNM 86, p. 405.

13. "Muon energy Loss at High Energy and Implications for Detector Design", J. J. Eastman and S C. Loken, BERK 87, p. 542.

14. "Electromagnetic Shower Background Associated with High energy μs", V. Innocente, BERK 87, p. 554.

15. "Reconstruction of Isolated Muons at the SSC", E. Nagy, BERK 87, p. 563.

16. "A General Purpose Toroidal Detector", B. G. Pope et al., ISABELLE, Proceedings of the 1981 Summer Workshop, BNL51443 (1981).
"Air Core Superconducting Toroids as Magnets Around Interior Points", L. W. Jones, BERK 87, p. 604.
B. Roe, private communication.

17. P. Bonanos, Princeton Plasma Physics Laboratory and J. N. Luton, Fusion Energy Division, Oak Ridge National Lab., private communication.

18. "Effect of Lepton Energy Resolution on Higgs Searches at the SSC", I. Hinchliffe and E. M. Wang, LBL-26302 (1988).

19. "Preliminary Results of a Reference Engineering Design Study for Hermetic Liquid Argon Calorimetry", T. Adams, et al., to be published in Proceedings of the SSC Workshop on Calorimetry, Alabama, 1989 (ALA 89).

20. E. M. Wang, private communication.

21. Electronics Working Group for Liquid Argon, to be published in ALA (89).

22. "The D0 Calorimeter", W. Cooper and "The NA34 (HELIOS) Calorimeter", D. Rahm at Workshop on Liquid Argon Calorimetry, Boulder (1988), Unpublished.

23. Scintillator Working Group to be published in ALA (89).

24. "CERES", Electron Pair Spectrometer. CERN/SPSC 88-25, p237.

25. Report of the Compact Detector Subgroup, BERK 87, p. 388.

26. D. Bintinger, private communication.

27. P. Bonanos, private communication.

Figures

1. The ZZ invariant mass distribution arising from Higgs decay and from the background process $q\bar{q} \rightarrow ZZ$. The distribution is shown for Higgs masses of 400, 600, and 800 GeV and top masses of 40 and 200 GeV. If the background process $gg \rightarrow ZZ$ were to be included, the background would be increased by a factor which is about 1.7 (1.6) for M_{ZZ} = 400(800) GeV (Ref. 2).

2. Di-lepton invariant mass distributions for various energy or momentum resolutions for leptons from Higgs bosons of 400 GeV/c^2 mass decaying into $ZZ \rightarrow 4l^{\pm}$ (Ref. 4).

3.a The reconstructed invariant mass distributions of dimuons from Higgs $\rightarrow$ ZZ, with 1 TeV Higgs and 200 GeV top for the L3 + 1 detector. The Higgs signal is clearly visible above the heavy quark background.

b The reconstructed invariant masses distributions of the same dimuons, as in Fig. 3.a, but with the momentum resolution of an iron toroid $\Delta P_T/P_T = .09 + .11\ P_T(\mathrm{GeV}/c)$ (Ref. 5).

4. Z-pair mass distributions for various energy or momentum resolutions for $H \rightarrow ZZ \rightarrow 4l^{\pm}$ for M_H = 400 GeV/c^2, along with the background from continuum ZZ production (Ref. 4).

5. Two-lepton angular acceptance for $Z \rightarrow ll$ from continuum $H^{\circ} \rightarrow ZZ$ events with Higgs masses of 300 and 800 GeV (Ref. 6).

6. Four-lepton angular acceptance for $ZZ \rightarrow llll$ from $H^{\circ} \rightarrow ZZ$ events with Higgs masses of 300 and 800 GeV (Ref. 6).

7. Forward-backward asymmetries in $pp \rightarrow Z'(\theta) + ... \rightarrow l^-l^+ + ...$ for $\sqrt{s}$ = 40 TeV, as function of rapidity. Here $M[Z(\theta)]$ = 1 TeV. θ is the model dependant mixing angle to be determined (Ref. 9).

8. Two lepton angular acceptance for $Z' \rightarrow ll$ for Z′ masses of 500, 1000 and 2000 GeV (Ref. 6).

9. The differential cross-section $d\sigma/dm$ for $pp \rightarrow l^+l^-X$ (l = e,μ) as a function of the lepton invariant mass M around the Z′-peak at 1 TeV, for a Z′ width of 25 GeV. Solid, dashed and dotted lines denote various models. Case (i) corresponds to a perfect momentum resolution, case (ii) to a momentum resolution of 15 percent (Ref. 10).

10. The same as in Fig. 9 but for the lepton asymmetry (Ref. 10).

11. Schematic view of the Large Solenoid Detector (Ref. 7).

12. The side view of the proposed L3 + 1 detector showing the precision muon detector at $\theta > 22°$ and the endcap toridal magnets (Ref. 8).

13. Momentum resolution for measurement of large-angle and forward-going muons in the Large Solenoid Detector (Ref. 7).

14. Momentum resolution as a function of polar angle and rapidity in the Large Solenoid Detector (Ref. 7).

15. The muon momentum resolution of the L3 + 1 detector as a function of the polar angle (Ref. 8).

16. 4π detector geometry with internal thin coil (Ref. 11).

17. Muon momentum measurement schemes for various magnetized-iron geometries (Ref. 12).

18. The resolution of the muon energy for various measurement strategies i.e. number of planes and angles (Ref. 12).

19. The probability of a clean muon hit unaccompanied by another charged particle after 1m of steel or uranium, as a function of muon energy (Ref. 13).

20. Simulated muon entering tracking volume with accompanying shower (Ref. 14).

21. Schematic of toroidal magnets for EMPACT. Figure shows central and end toroids with one coil sectioned to show interior tracking volume.

22. Side and beam view of EMPACT detector.

23. Engineering model of liquid argon calorimeter suitable for EMPACT (Ref. 19).

24. 100 GeV pion and electron resolution as a function of rapidity, showing effects of walls and supports in model shown in Fig. 23 (Ref. 19).

25. Two lepton angular acceptance for both Ws decaying to $l\nu$ from continuum W pair events for P_TWs of 100, 300, and 500 GeV/c.

26. Section of one quadrant of idealized toroidal current arrangement to define parameters in Appendix A. Note several possibilities of division of central from end coils.

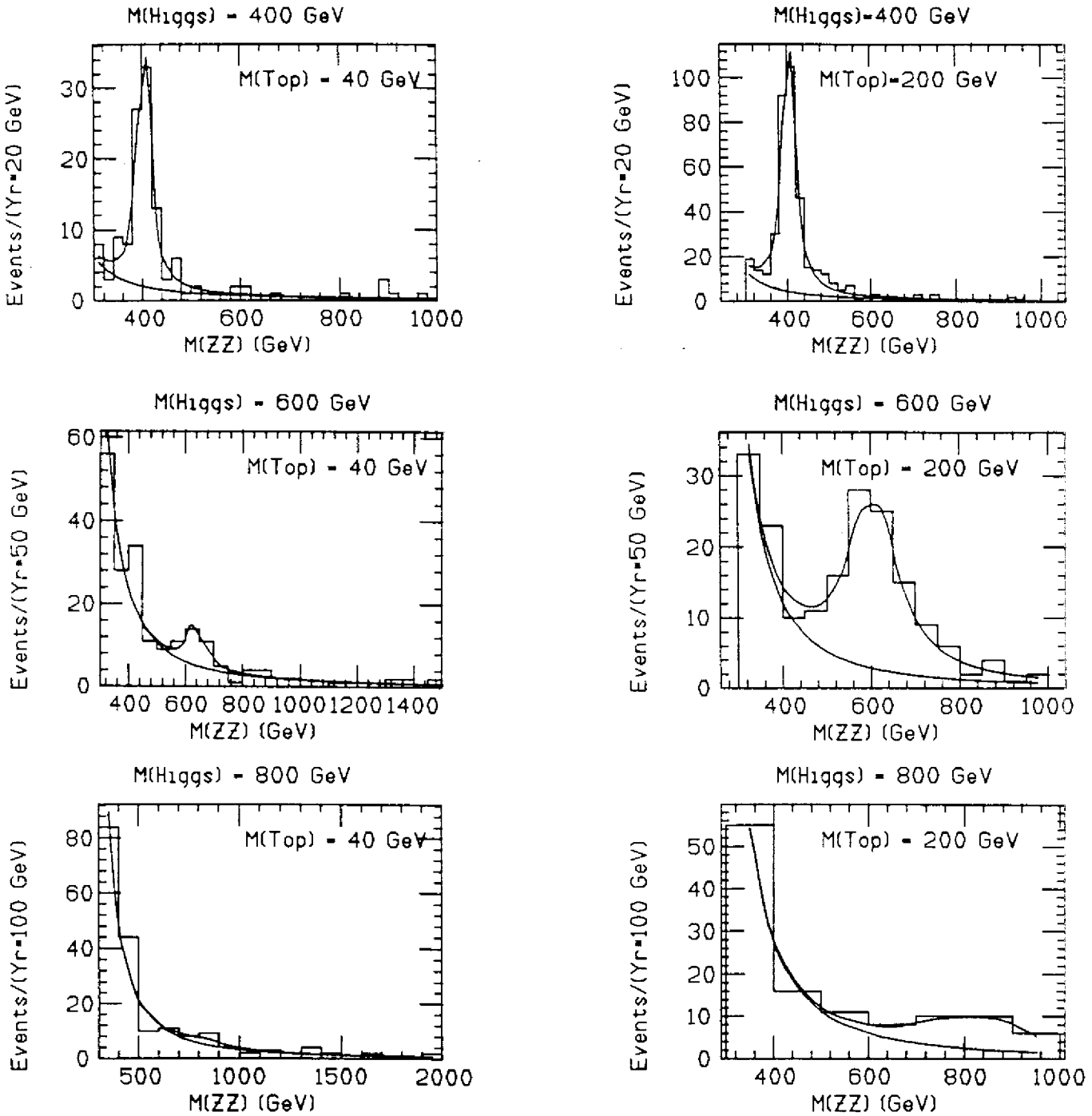
M(Higgs) = 400 GeV
M(Top) = 40 GeV
Events/(Yr=20 GeV)
M(ZZ) (GeV)
M(Higgs)=400 GeV
M(Top)=200 GeV
Events/(Yr=20 GeV)
M(ZZ) (GeV)
M(Higgs) = 600 GeV
M(Top) = 40 GeV
Events/(Yr=50 GeV)
M(ZZ) (GeV)
M(Higgs) = 600 GeV
M(Top) = 200 GeV
Events/(Yr=50 GeV)
M(ZZ) (GeV)
M(Higgs) = 800 GeV
M(Top) = 40 GeV
Events/(Yr=100 GeV)
M(ZZ) (GeV)
M(Higgs) = 800 GeV
M(Top) = 200 GeV
Events/(Yr=100 GeV)
M(ZZ) (GeV)

Figure 1

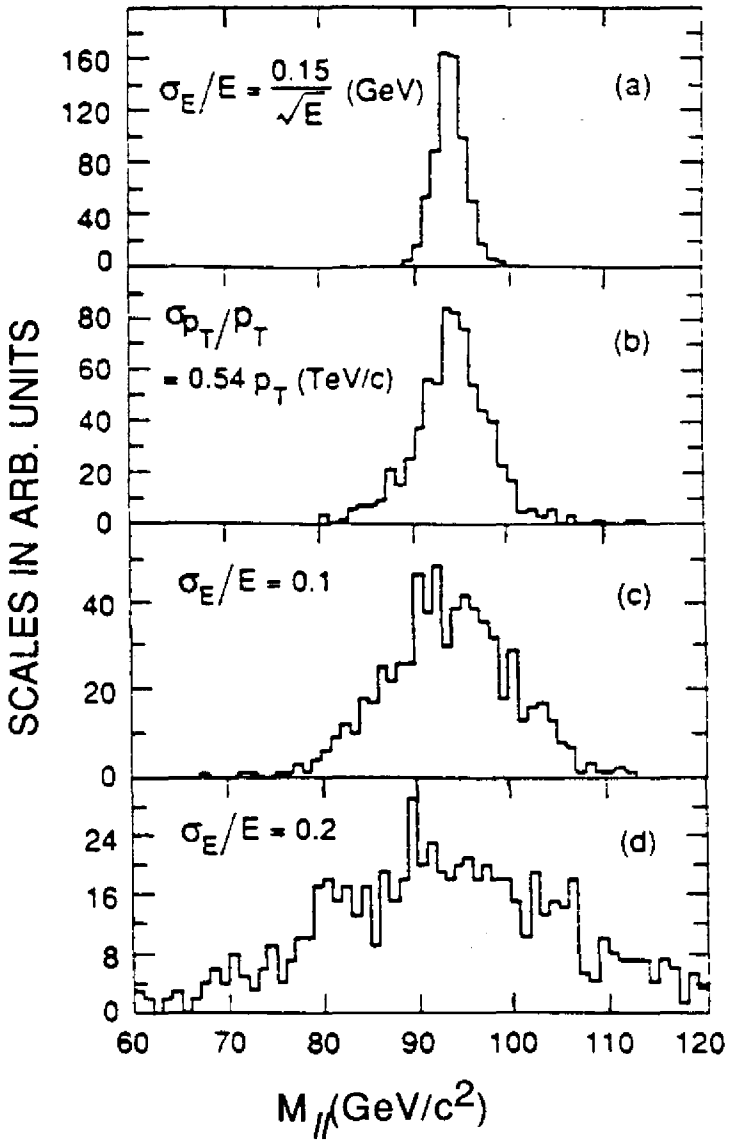
SCALES IN ARB. UNITS
$\sigma_E/E = \frac{0.15}{\sqrt{E}}$ (GeV)
(a)
σ_{p_T}/p_T
$= 0.54\ p_T$ (TeV/c)
(b)
$\sigma_E/E = 0.1$
(c)
$\sigma_E/E = 0.2$
(d)
M_{ll}(GeV/c^2)

Figure 2

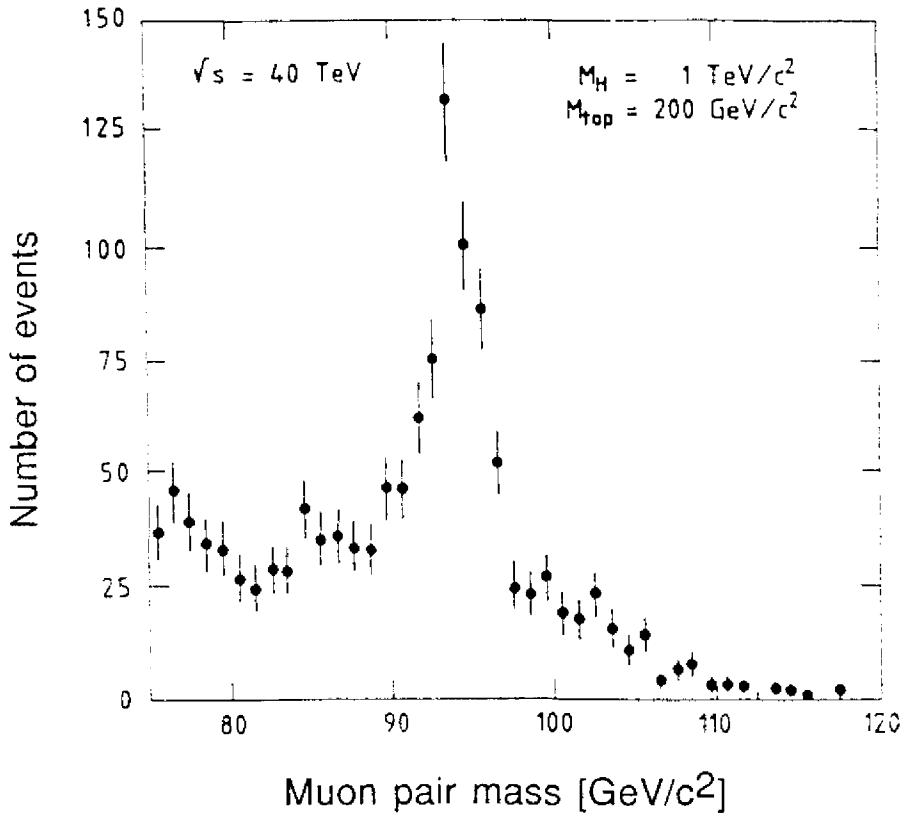

Figure 3a

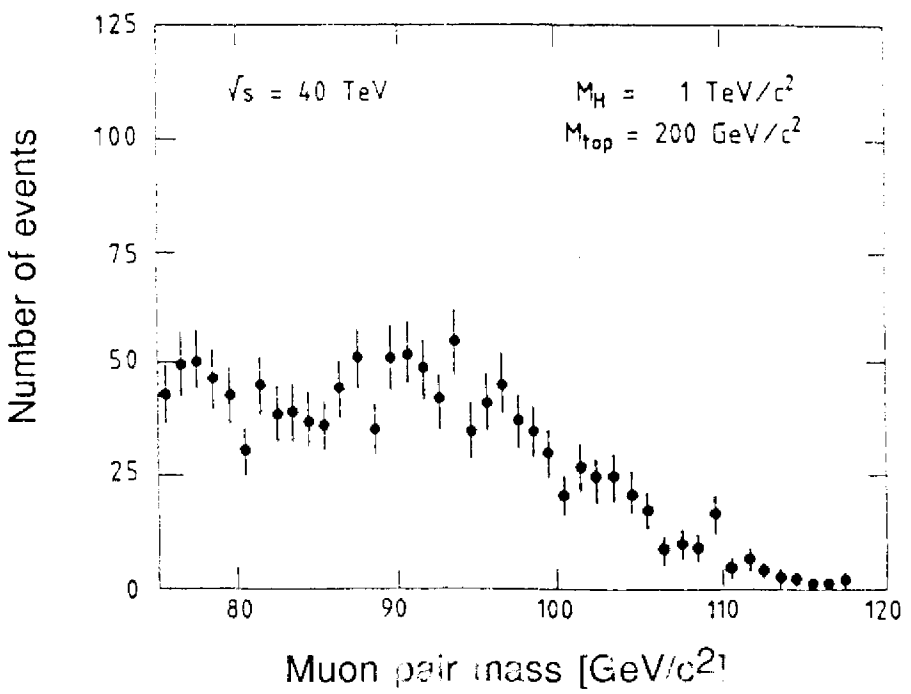

Figure 3b

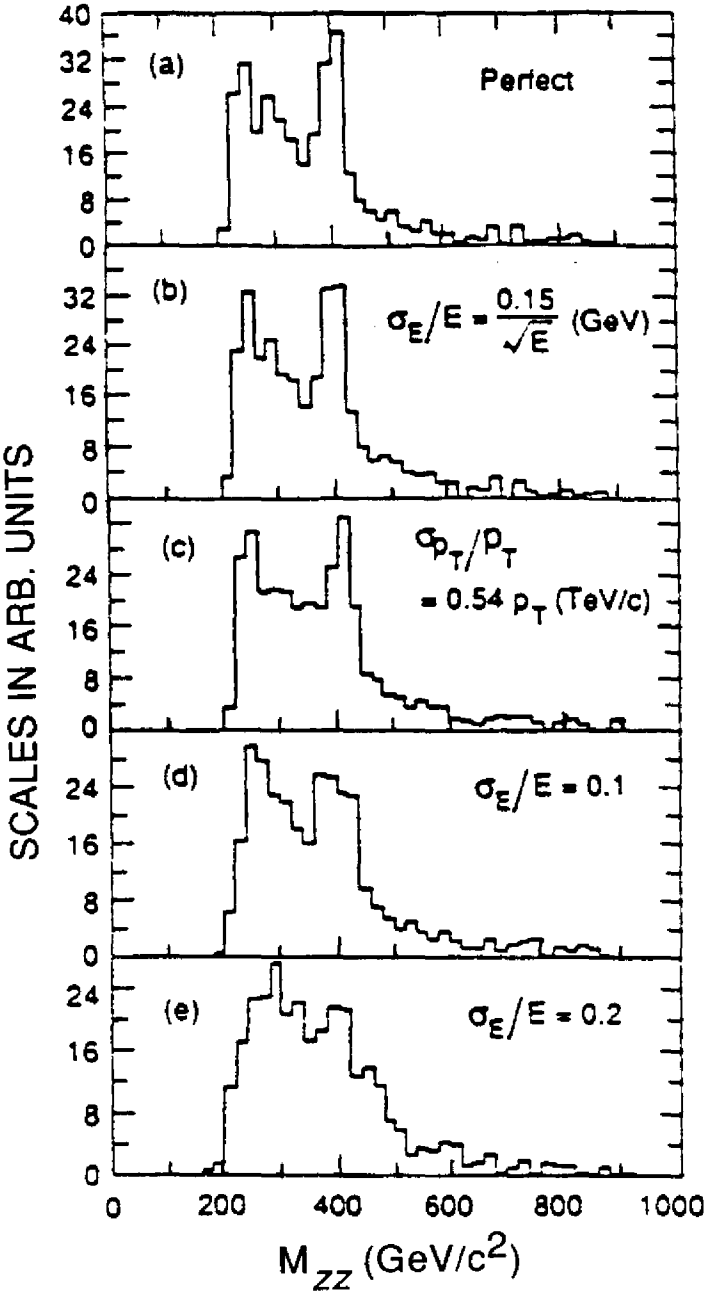
(a)
Perfect
(b)
$\sigma_E/E = \frac{0.15}{\sqrt{E}}$ (GeV)
(c)
σ_{p_T}/p_T
$= 0.54\ p_T$ (TeV/c)
(d)
$\sigma_E/E = 0.1$
(e)
$\sigma_E/E = 0.2$
SCALES IN ARB. UNITS
M_{ZZ} (GeV/c^2)
0
200
400
600
800
1000

Figure 4

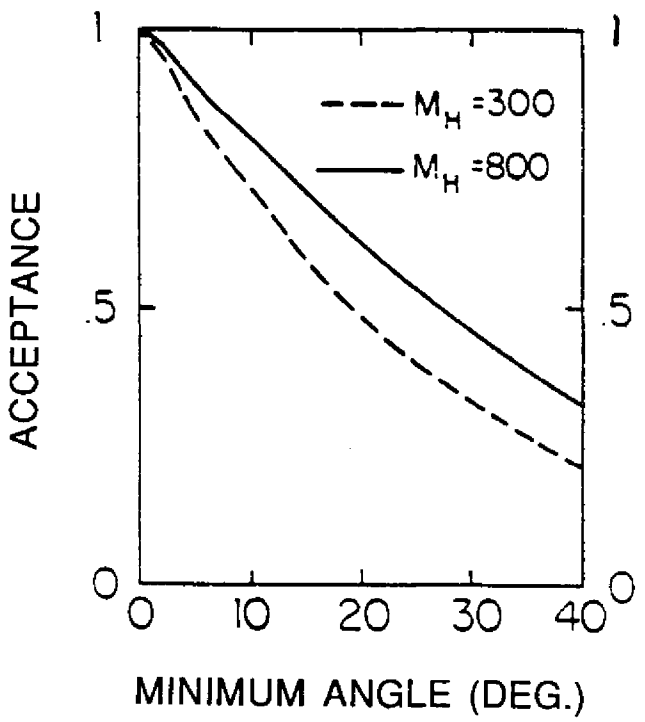
1
.5
0
1
.5
0
0
10
20
30
40
ACCEPTANCE
MINIMUM ANGLE (DEG.)
M_H =300
M_H =800

Figure 5

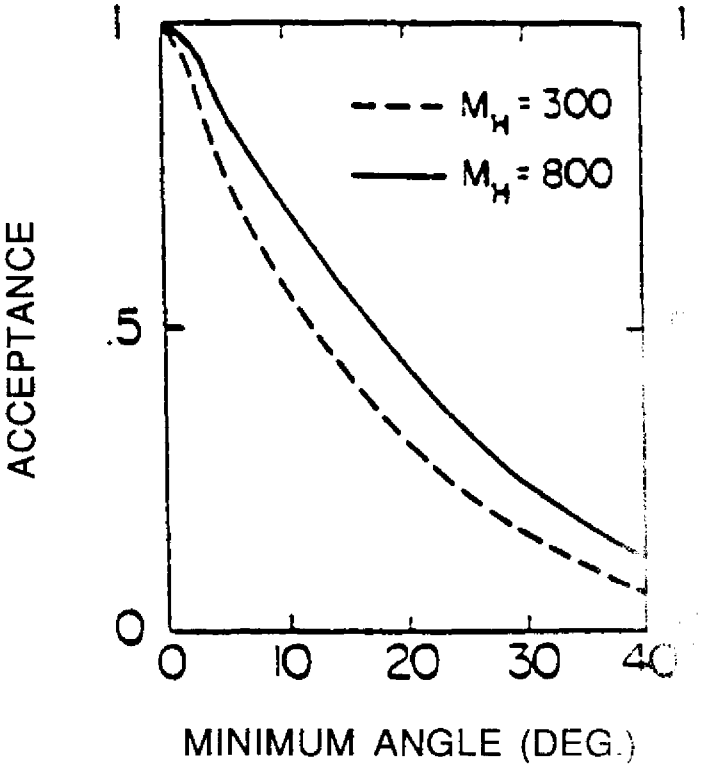

Figure 6

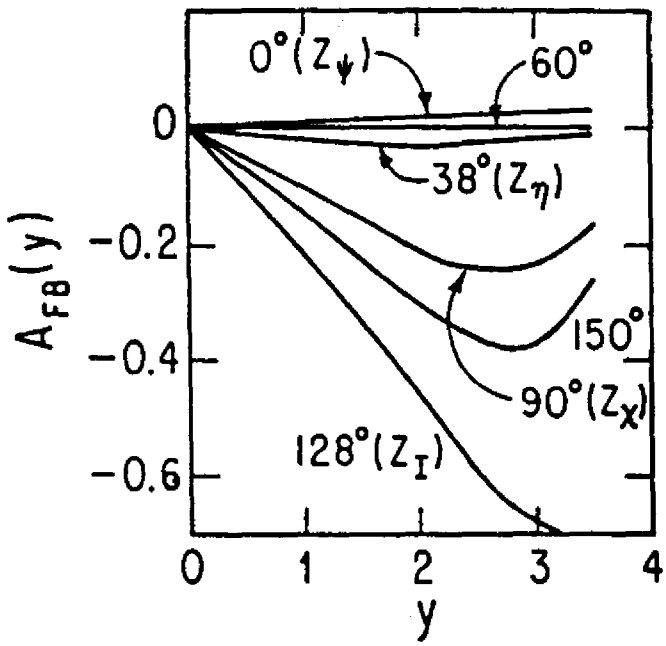

Figure 7

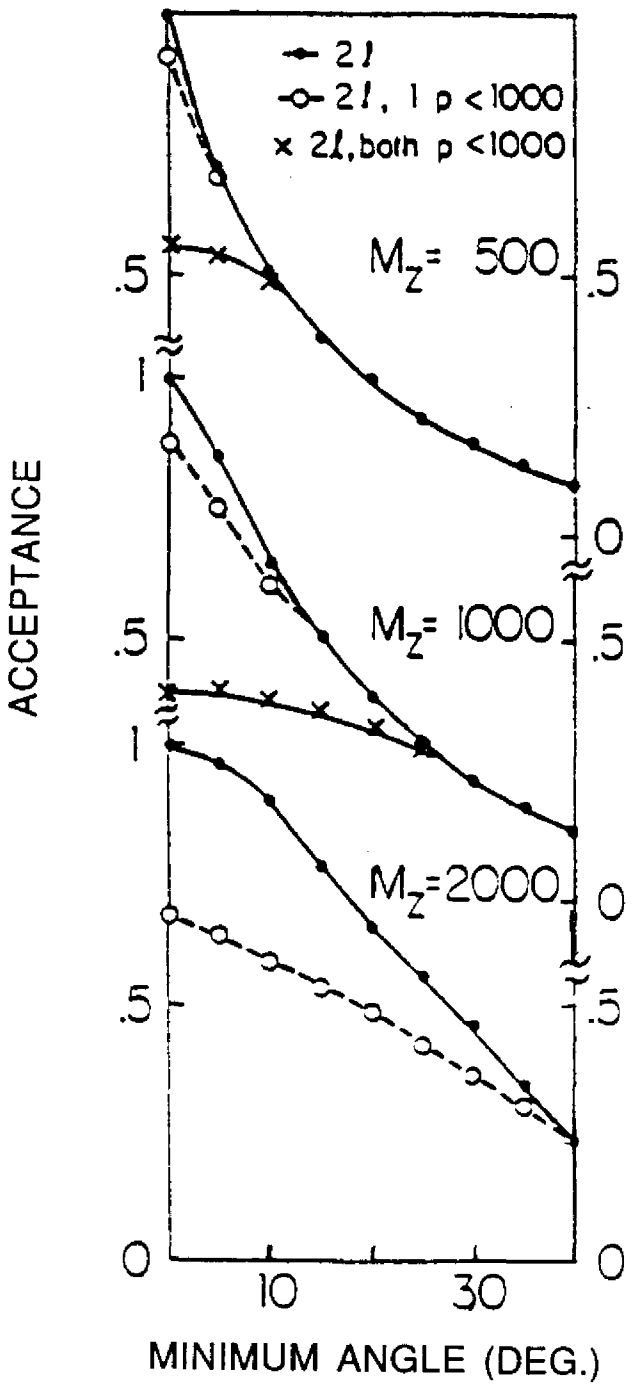
2l
2l, 1 p <1000
× 2l, both p <1000
M_Z= 500
M_Z= 1000
M_Z=2000
ACCEPTANCE
MINIMUM ANGLE (DEG.)
.5
1
0
10
30

Figure 8

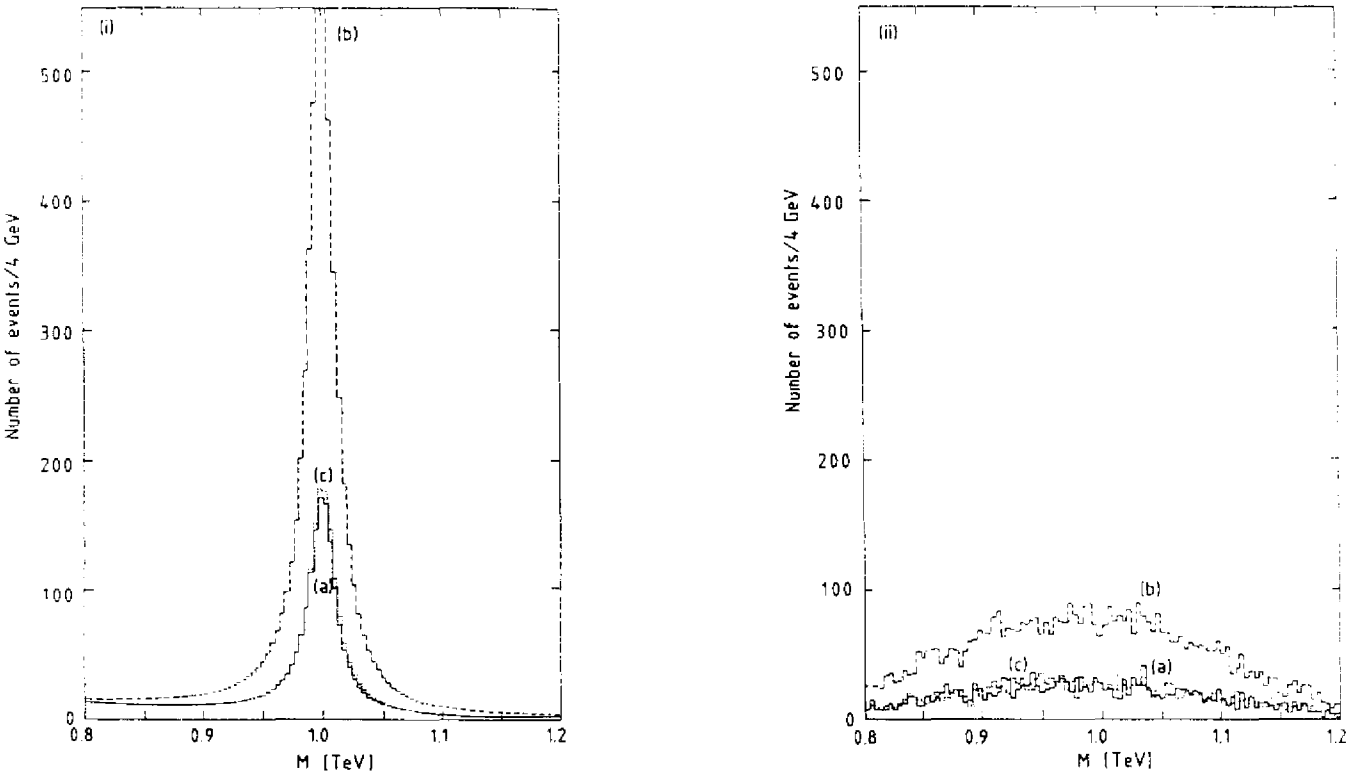
(i)
(b)
(c)
(a)
Number of events/4 GeV
M [TeV]
(ii)
(b)
(c)
(a)
Number of events/4 GeV
M [TeV]

Figure 9

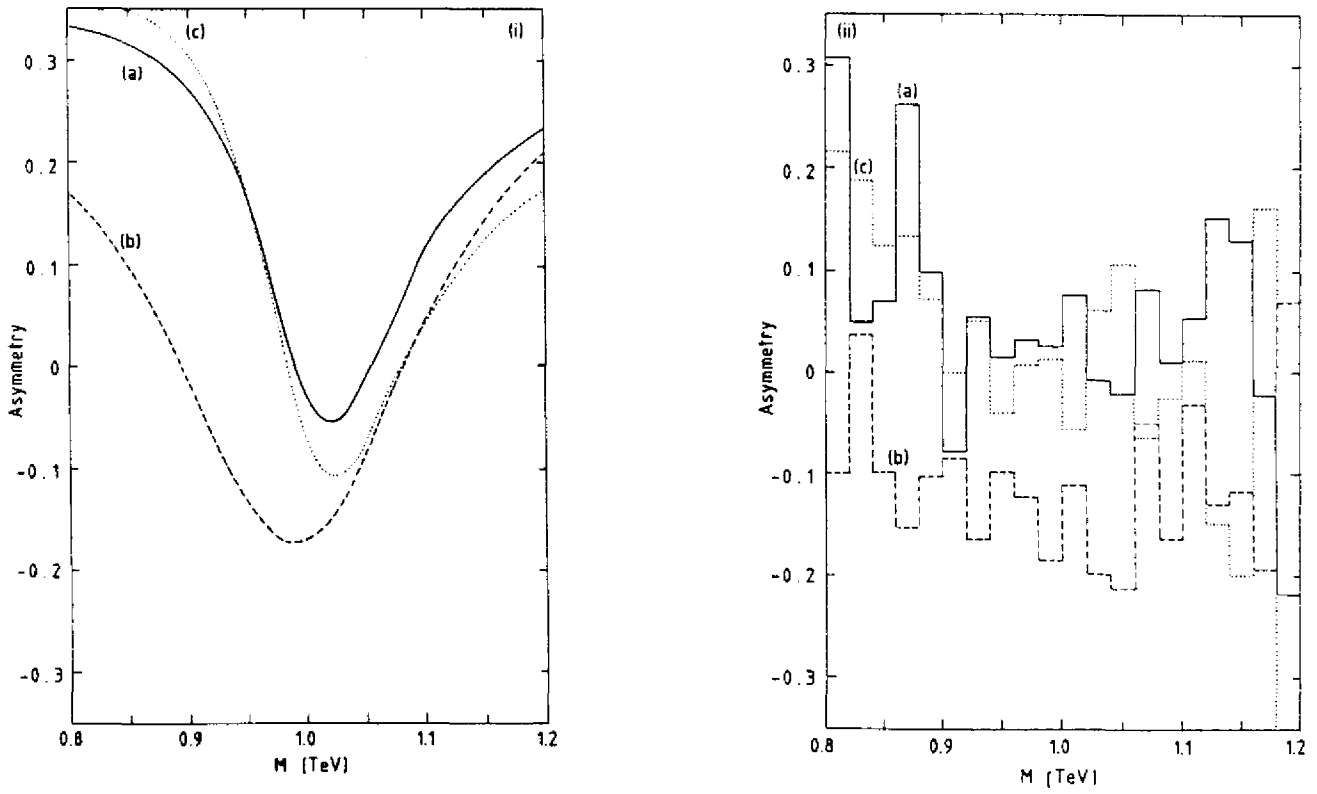

Figure 10

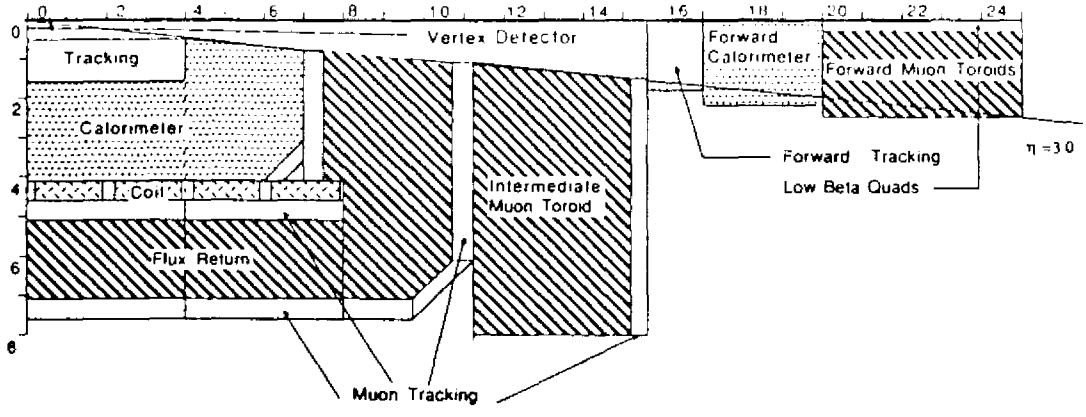
0
2
4
6
8
10
12
14
16
18
20
22
24
Vertex Detector
Tracking
Calorimeter
Coil
Flux Return
Intermediate
Muon Toroid
Forward
Calorimeter
Forward Muon Toroids
Forward Tracking
Low Beta Quads
η = 3.0
Muon Tracking

Figure 11

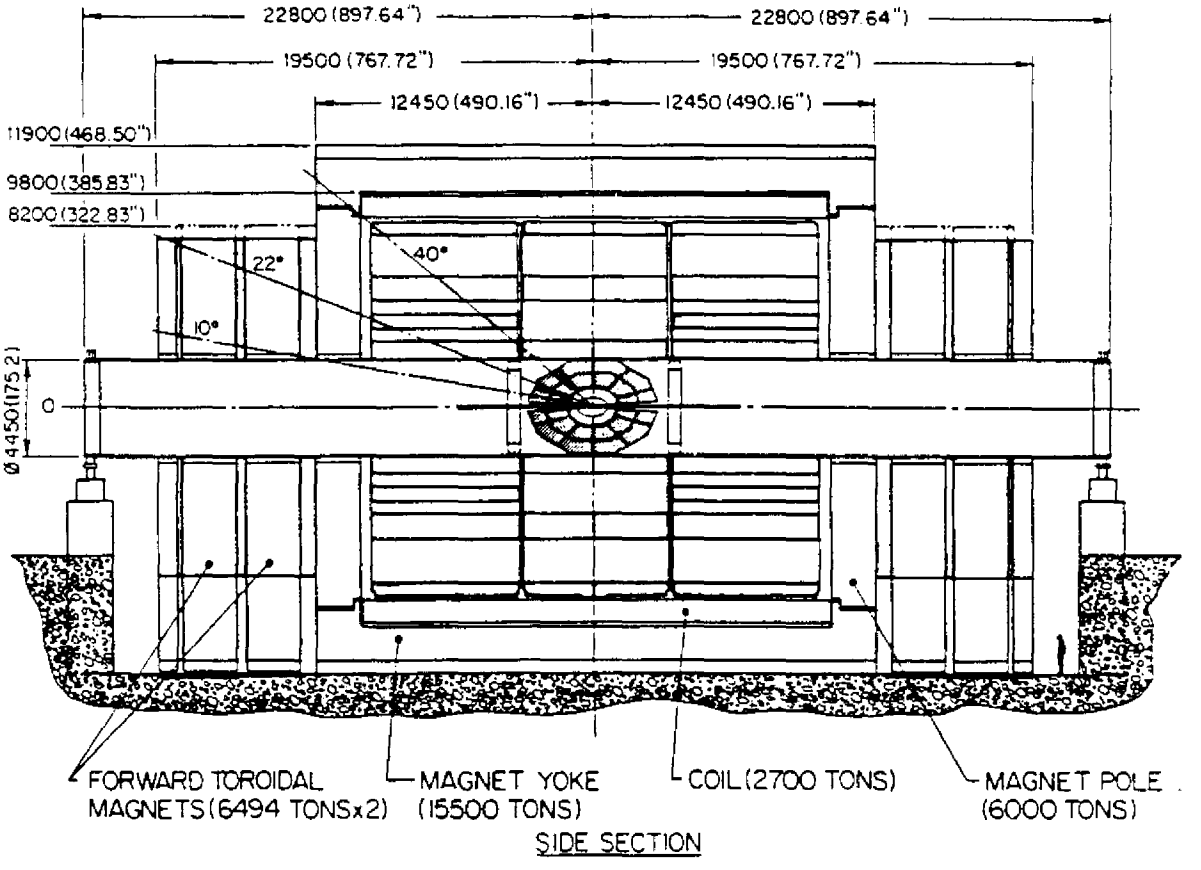
22800 (897.64")
22800 (897.64")
19500 (767.72")
19500 (767.72")
12450 (490.16")
12450 (490.16")
11900 (468.50")
9800 (385.83")
8200 (322.83")
22°
40°
10°
Ø4450 (175.2)
0
FORWARD TOROIDAL MAGNETS (6494 TONS x 2)
MAGNET YOKE (15500 TONS)
COIL (2700 TONS)
MAGNET POLE (6000 TONS)
SIDE SECTION

Figure 12

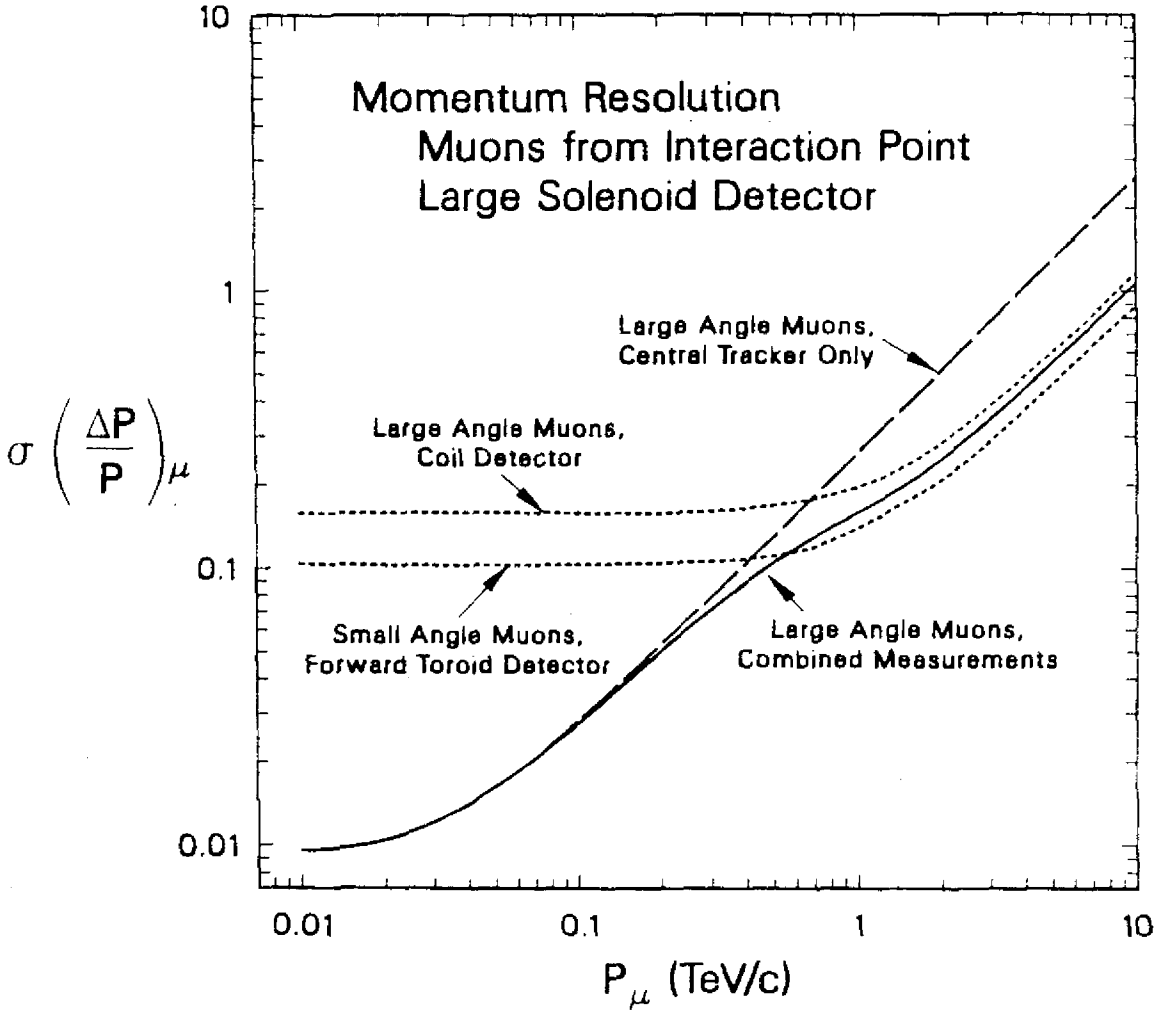
Momentum Resolution
Muons from Interaction Point
Large Solenoid Detector
Large Angle Muons,
Central Tracker Only
Large Angle Muons,
Coil Detector
Small Angle Muons,
Forward Toroid Detector
Large Angle Muons,
Combined Measurements
$\sigma\left(\frac{\Delta P}{P}\right)_\mu$
10
1
0.1
0.01
0.01
0.1
1
10
P_μ (TeV/c)

Figure 13

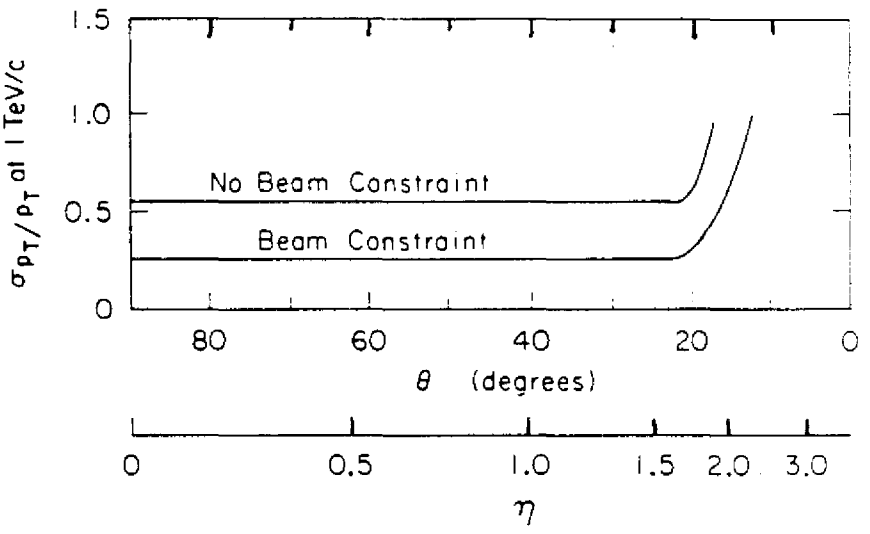
1.5
1.0
0.5
0
σ_{p_T}/p_T at 1 TeV/c
No Beam Constraint
Beam Constraint
80
60
40
20
0
θ (degrees)
0
0.5
1.0
1.5
2.0
3.0
η

Figure 14

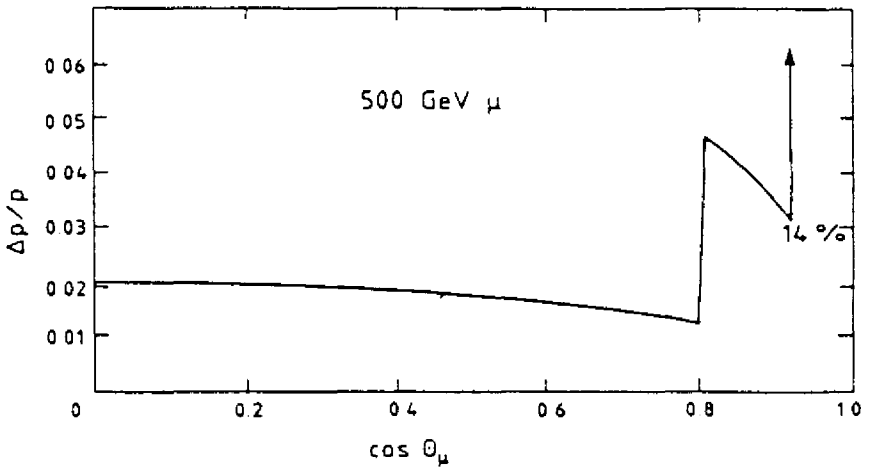

Figure 15

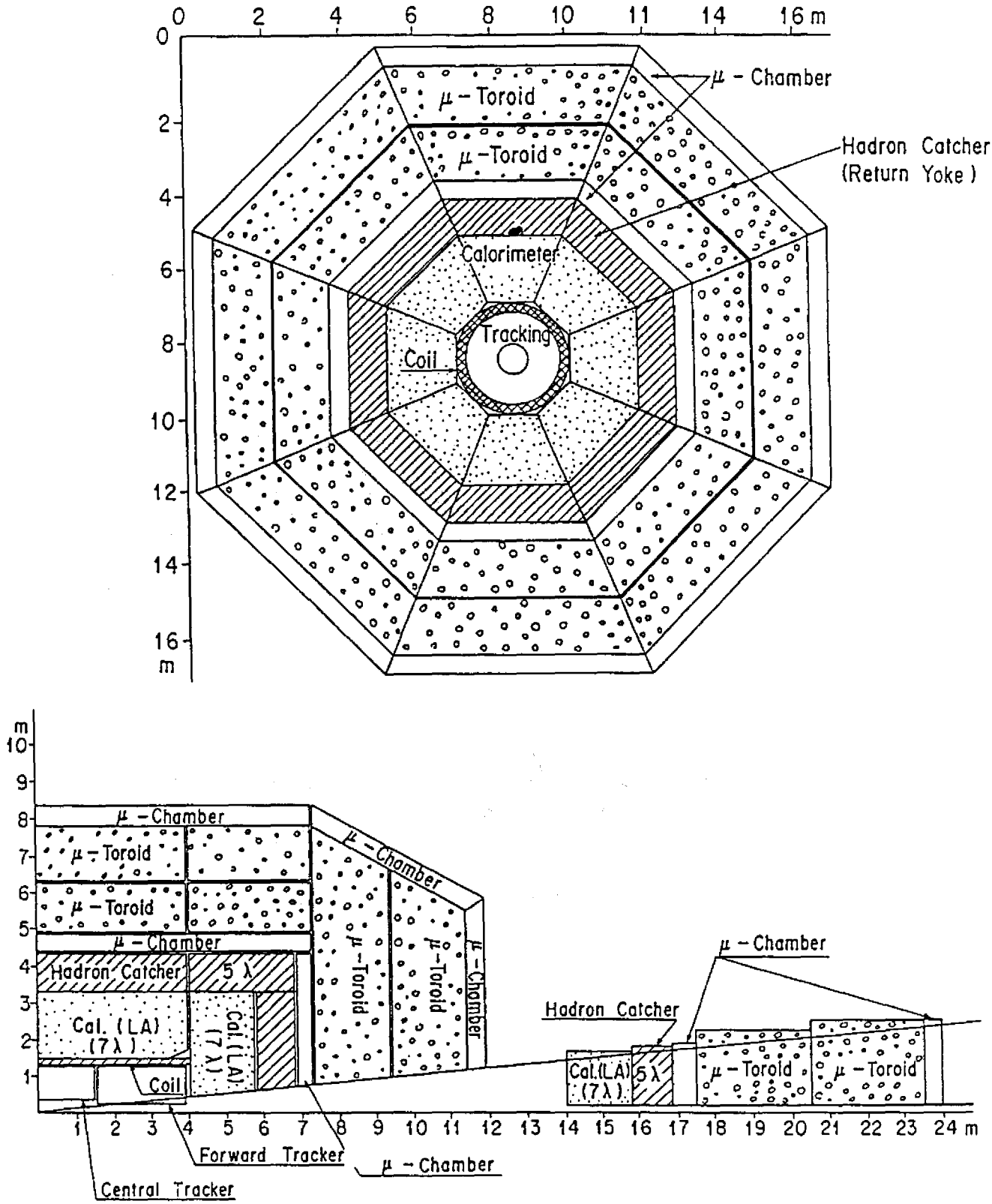
0 2 4 6 8 10 11 14 16 m
μ - Chamber
μ - Toroid
μ - Toroid
Hadron Catcher
(Return Yoke)
Calorimeter
Tracking
Coil
m
μ - Chamber
μ - Toroid
μ - Toroid
μ - Chamber
Hadron Catcher
5 λ
Cal. (LA)
(7 λ)
Coil
μ - Toroid
μ - Toroid
μ - Chamber
μ - Chamber
Hadron Catcher
Cal.(LA)
(7 λ)
5 λ
μ - Toroid
μ - Toroid
1 2 3 4 5 6 7 8 9 10 11 12 13 14 15 16 17 18 19 20 21 22 23 24 m
Forward Tracker
μ - Chamber
Central Tracker

Figure 16

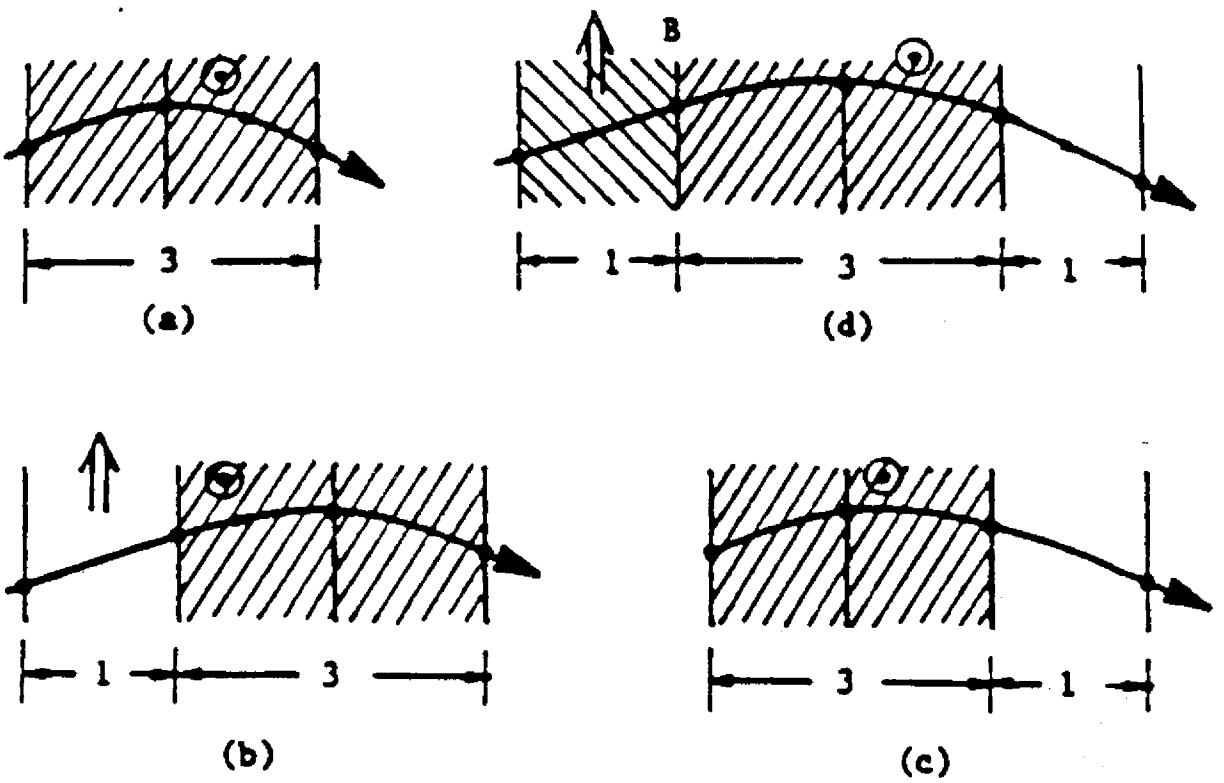

Figure 17

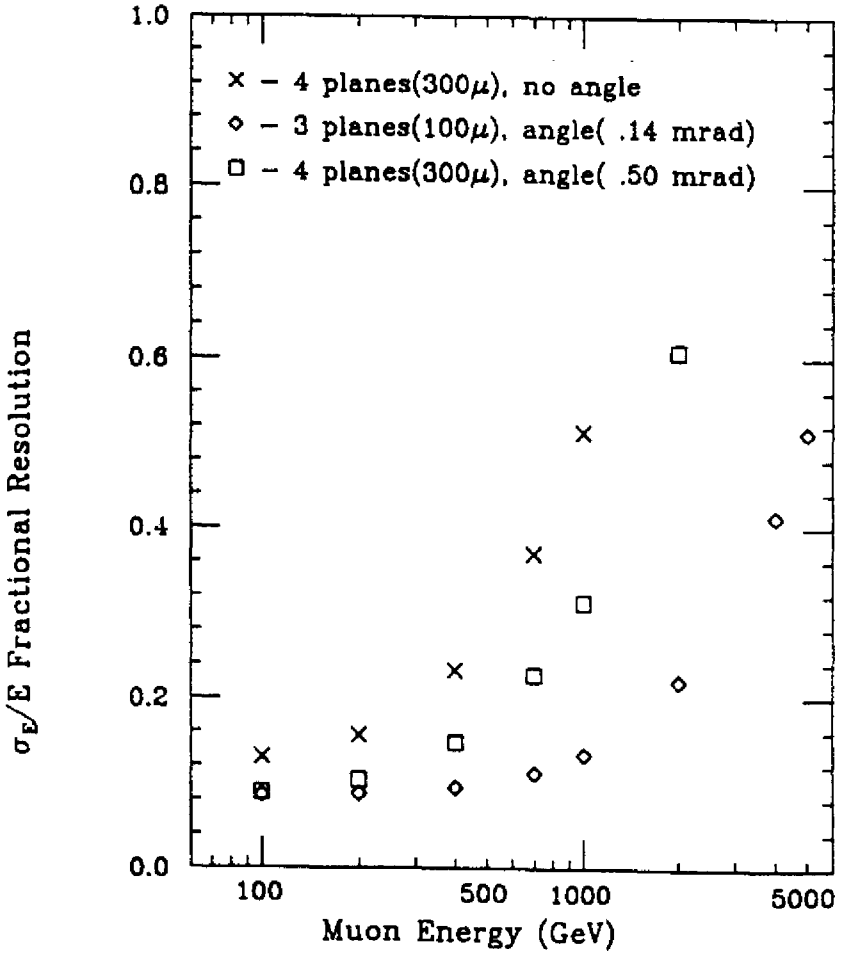
× – 4 planes(300μ), no angle
◇ – 3 planes(100μ), angle(.14 mrad)
□ – 4 planes(300μ), angle(.50 mrad)
1.0
0.8
0.6
0.4
0.2
0.0
σE/E Fractional Resolution
100
500
1000
5000
Muon Energy (GeV)

Figure 18

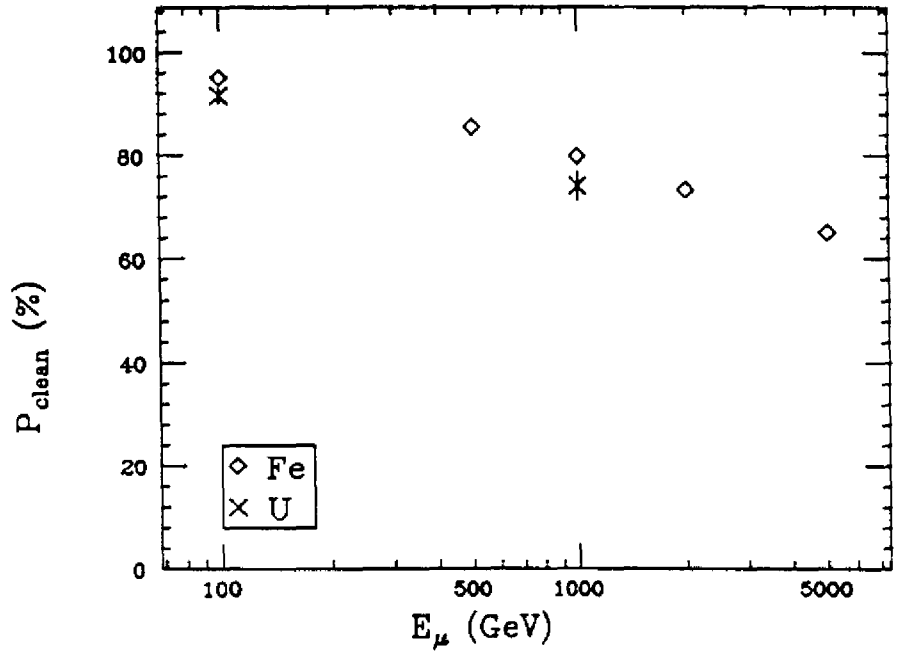

Figure 19

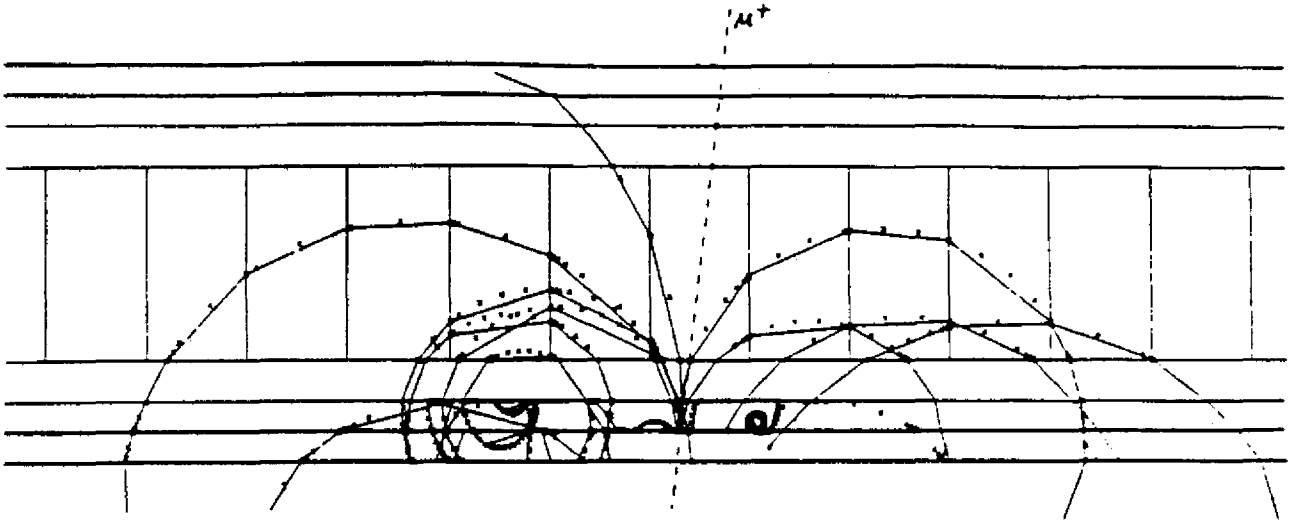

Figure 20

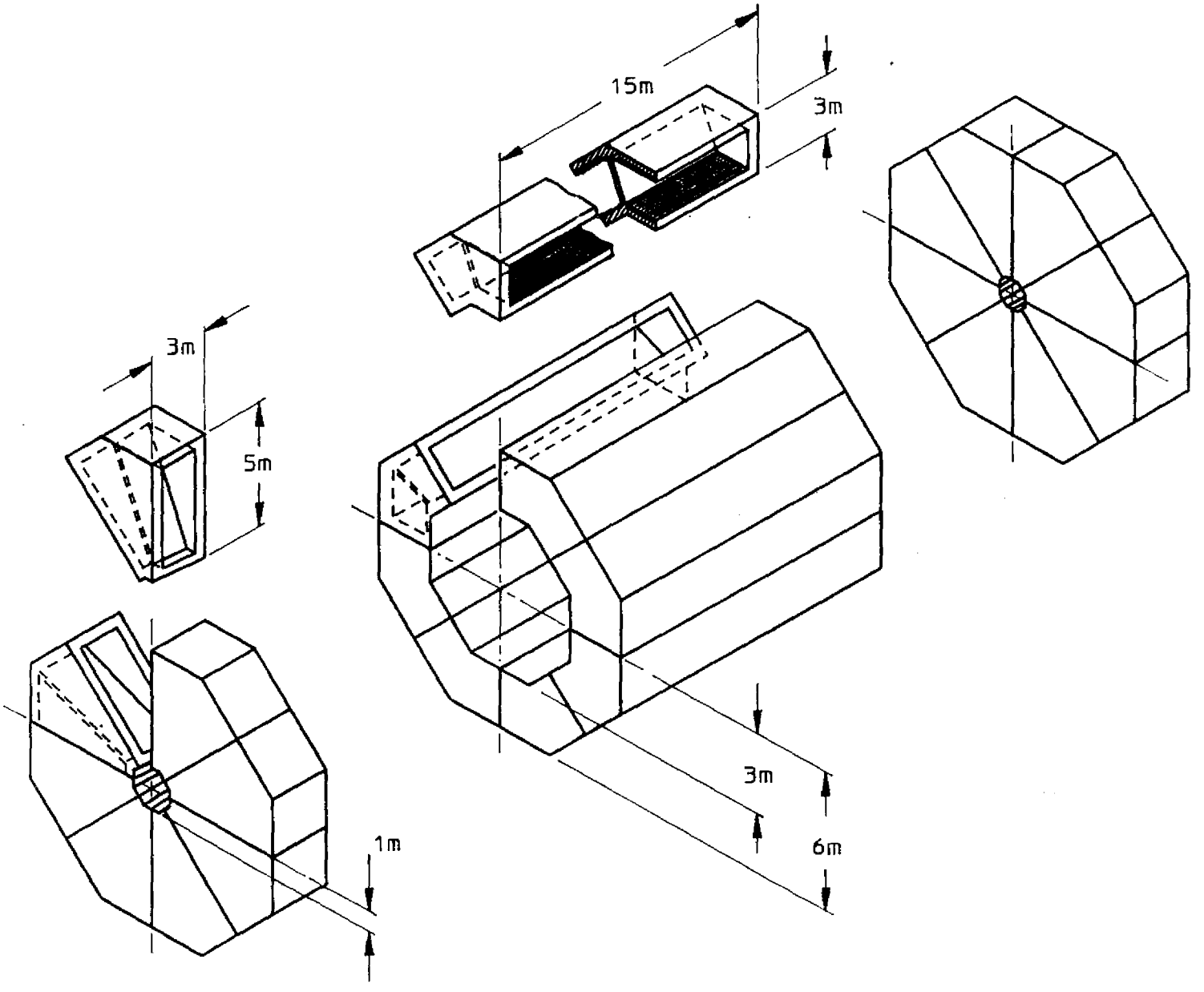

Figure 21

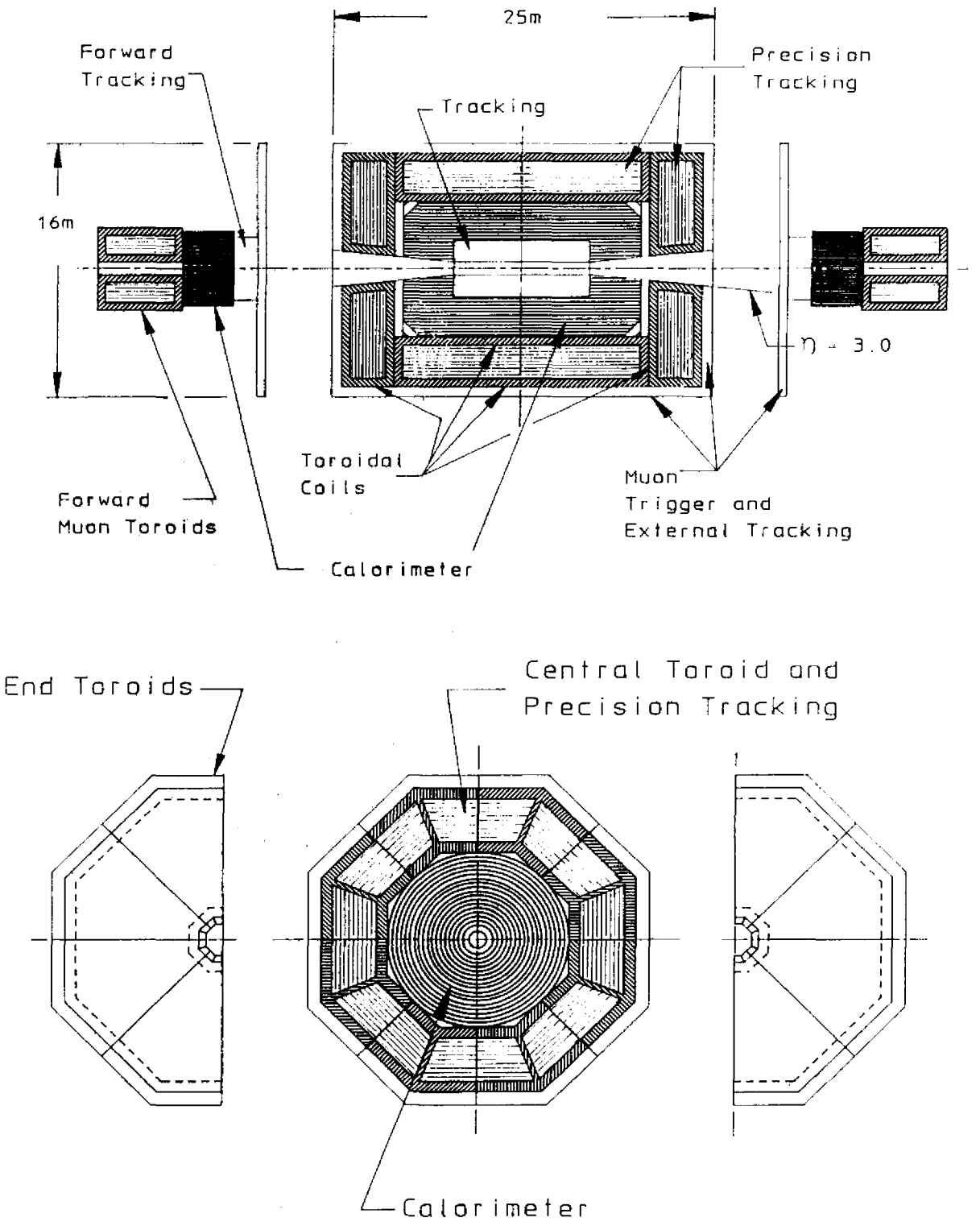
25m
Forward
Tracking
Precision
Tracking
Tracking
16m
η = 3.0
Toroidal
Coils
Muon
Trigger and
External Tracking
Forward
Muon Toroids
Calorimeter
End Toroids
Central Toroid and
Precision Tracking
Calorimeter

Figure 22

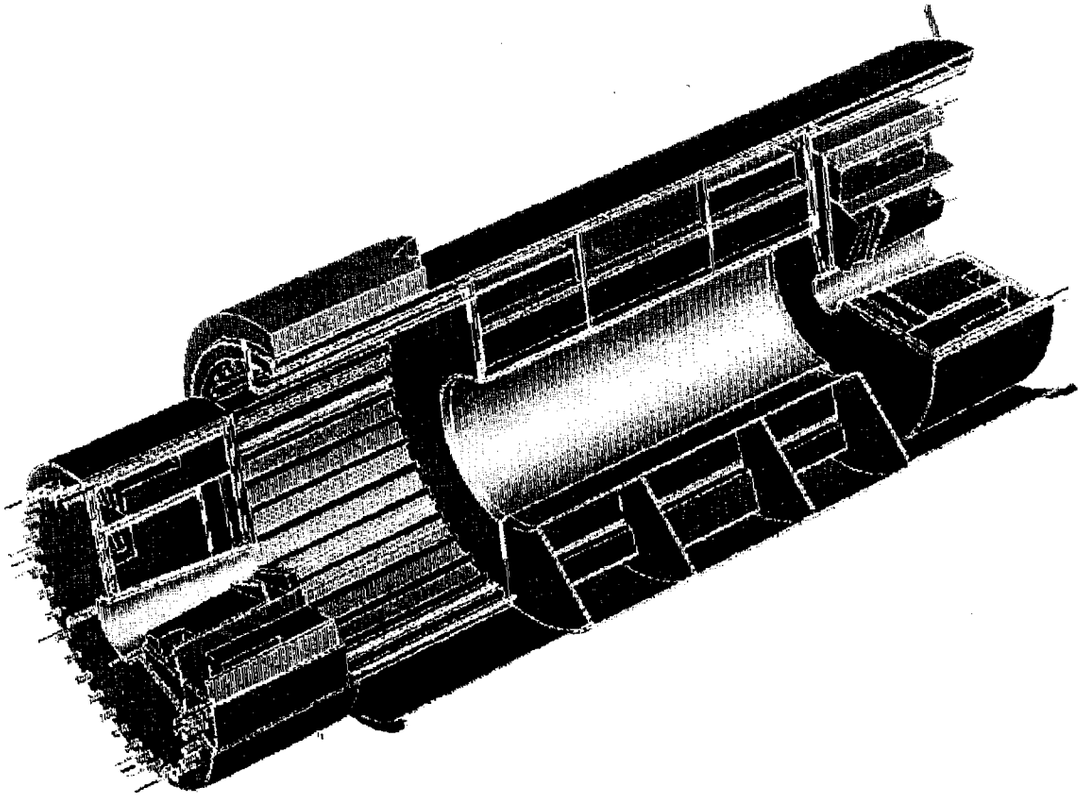

Figure 23

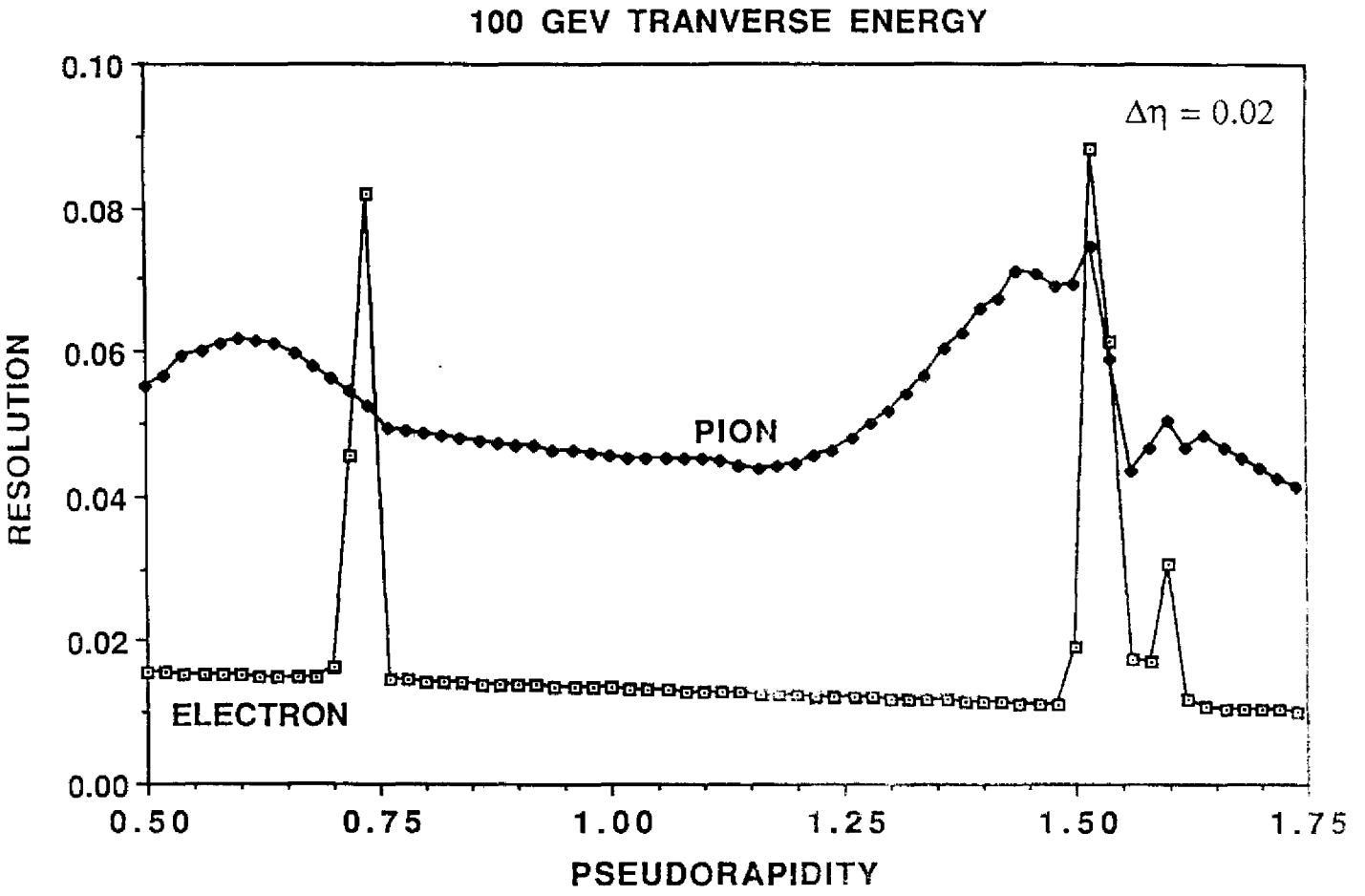
100 GEV TRANVERSE ENERGY
Δη = 0.02
PION
ELECTRON
RESOLUTION
0.10
0.08
0.06
0.04
0.02
0.00
0.50
0.75
1.00
1.25
1.50
1.75
PSEUDORAPIDITY

Figure 24

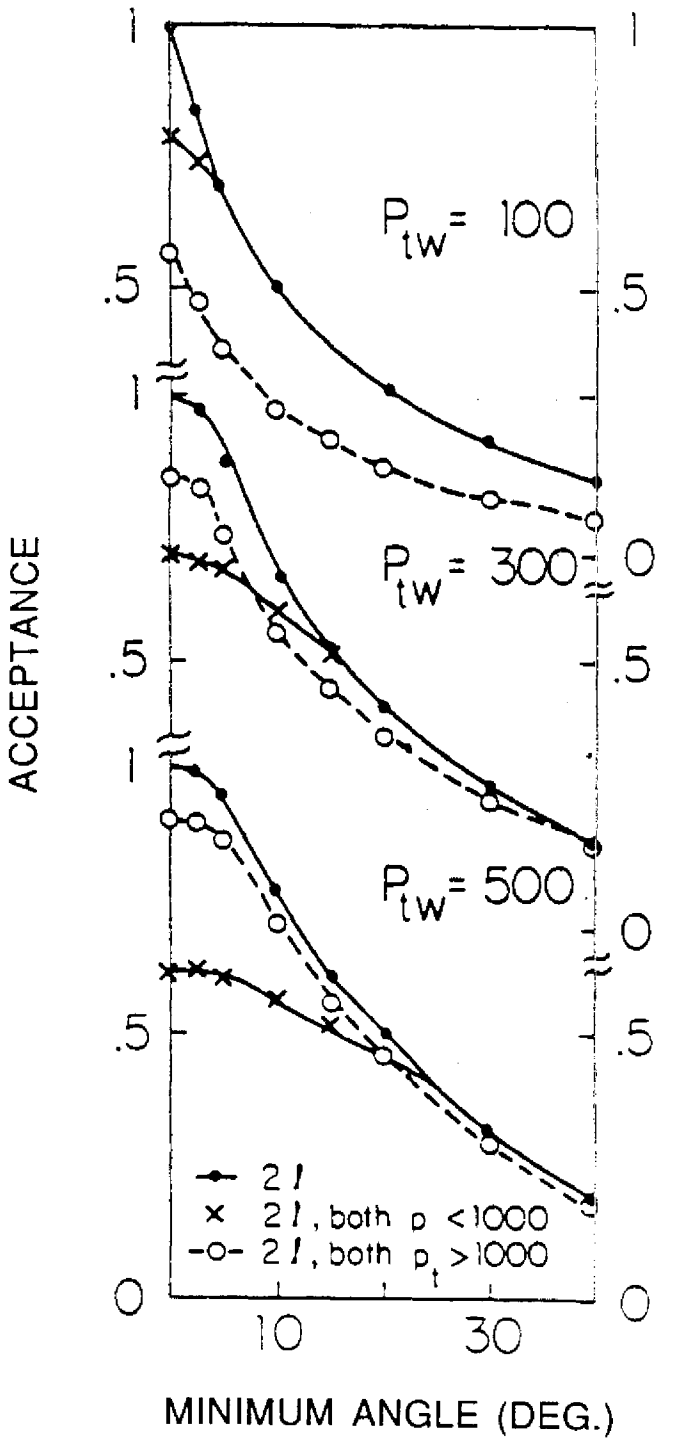
ACCEPTANCE
MINIMUM ANGLE (DEG.)
P_{tw}= 100
P_{tw}= 300
P_{tw}= 500
2 l
2 l, both p <1000
2 l, both p_t >1000
1
.5
0
10
30

Figure 25

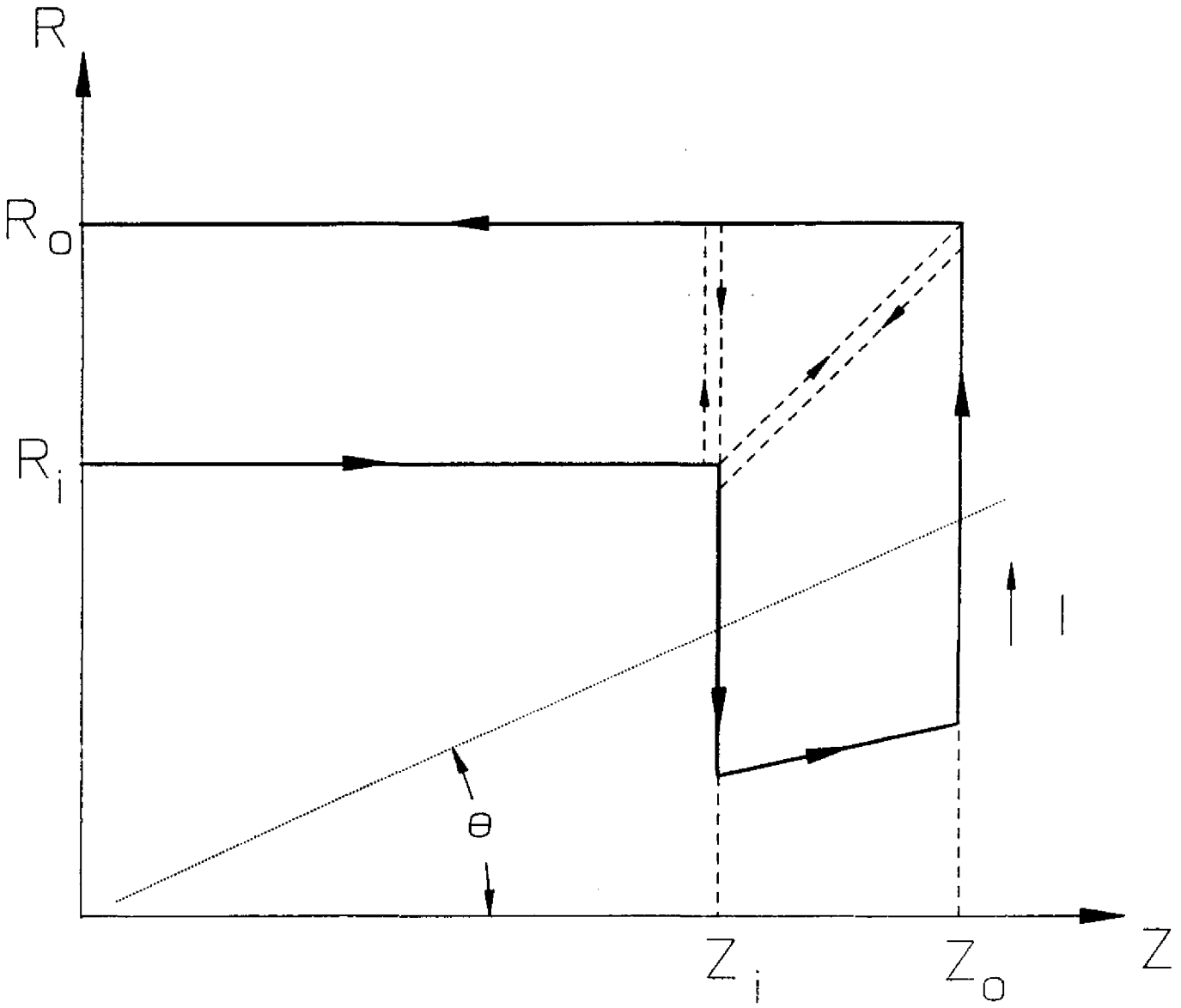

Figure 26